Improved Power Production Efficiency of Hydrothermal Reservoirs Using Downhole Pumps

Daniel Drader

Faculty of Mechanical and Industrial Engineering
University of Iceland
2011

IMPROVED POWER PRODUCTION EFFICIENCY OF HYDROTHERMAL RESERVOIRS USING DOWNHOLE PUMPS

Daniel Drader

60 ECTS thesis submitted in partial fulfillment of a
Magister Scientiarum degree in Mechanical Engineering

Advisors
Magnús Þór Jónsson
Halldór Pálsson

Faculty Representative
Marta Rós Karlsdóttir

Faculty of Mechanical and Industrial Engineering
School of Engineering and Natural Sciences
University of Iceland
Reykjavik, 09 2011

Improved Power Production Efficiency of Hydrothermal Reservoirs Using Downhole Pumps
Improved Geothermal Power Production Using Pumps
60 ECTS thesis submitted in partial fulfillment of a M.Sc. degree in Mechanical Engineering

Faculty of Mechanical and Industrial Engineering
School of Engineering and Natural Sciences
University of Iceland
VR II, Hjarðarhaga 2-6
107, Reykjavik
Iceland

Telephone: 525 4632

Bibliographic information:
Daniel Drader, 2011, Improved Power Production Efficiency of Hydrothermal Reservoirs Using Downhole Pumps, M.Sc. thesis, Faculty of Mechanical and Industrial Engineering, University of Iceland.

Printing: Háskólaprent, Fálkagata 2, 107 Reykjavík
Reykjavik, Iceland, 09 2011

Abstract

This study investigates the potential gains in power production of high temperature geothermal fields through the use of electric submersable pumps (ESP) in reservoirs currently being exploited using two phase flashing systems. The use of downhole pumps is predicted to have two benefits, the first being an increase in mass flow per well which could potentially reduce drilling costs. The second benefit the pumps can provide is the prevention of exergy loss to the flashing process which occurs under conventional two phase wellbore flow. It was predicted that the power consumed by the pump can be recovered at the power plant resulting in higher energy output for each wellbore drilled. In addition to increased power production the study investigates the economic benefits of increasing the mass flow from each well to determine if the pumps maintainence costs and power consumption could be offset to yield higher returns for plant owners. A brief summary of potential social and enviromental benefits for a closed loop approach is also discussed as the author predicts these may become of increasing importance in coming years.

Contents

List of Figures

List of Tables

Nomenclature

A	*Cross Sectional Area* (m^2)
D	*Inner Pipe Diameter* (m)
$\dot{E}_C$	*Exergy Distruction Rate for a Condenser* (kW)
$\dot{E}_{DS}$	*Exergy Distruction Rate for a Throttling Valve* (kW)
$\dot{E}_{IHE}$	*Exergy Distruction Rate for a Recouperator* (kW)
$\dot{E}_R$	*Exergy Distruction Rate for Reinjection* (kW)
$\dot{E}_T$	*Exergy Distruction Rate for a Turbine* (kW)
f	*Friction Factor for a surface*
Fr	*Froude Number*
g_c	*Gravitational Constant* (m/s^2)
H	*Height of Producing Formation* (m)
h_n	*Enthalpy* (kJ/kg) *at point* n
h_{ns}	*Enthalpy* (kJ/kg) *at point* n *assuming an Isentropic process*
h_{nL}	*Enthalpy* (kJ/kg) *of a liquid at point* n
Φ^2	*Friedel Correction Factor*
k	*Permeability* (m^2)
k_e	*Eötvös constant* ($JK^{-1}mol^{-\frac{2}{3}}$)
L	*Length* (m)
$\dot{m}_n$	*Mass Flow* (kg/s) *at point* n
P	*Pressure* (kPa)
P_D	*Dimensionless Pressure*
P_i	*Initial Reservior Pressure* (kPa)

$\dot{Q}_C$	*Condenser Cooling Capacity (kW)*
$\dot{Q}_{IHE}$	*Regenerator Capacity (kW)*
r	*Drainage Radius (m)*
r_e	*Reservior Boundary Radius (m)*
r_{eD}	*Dimensionless Radius*
r_w	*Wellbore Radius (m)*
S	*Slip Ratio (Dimensionless)*
s_0	*Dead State Entropy (kJ/kg K)*
s_n	*Specific Entropy at point n (kJ/kg K)*
s_{nL}	*Specific Entropy of a liquid at point n (kJ/kg K)*
T	*Temperature (°C)*
t	*Time (s)*
T_0	*Dead State Temperature (°K)*
η_T	*Turbine Efficiency (%)*
η_P	*Pump Efficiency (%)*
μ	*Viscosity* ($Pa \cdot s$)
ρ	*Density* (kg/m^3)
ρ_g	*Gas Density* (kg/m^3)
ρ_l	*Liquid Density* (kg/m^3)
ρ_m	*Mixture Density* (kg/m^3)
σ	*Surface Tension (mN/m)*
θ	*Wellbore Inclination from Vertical (°)*
v	*Velocity (m/s)*
V	*Molar Volume (ml/mol)*
$\dot{W}_T$	*Turbine Work (kW)*
We	*Weber Number*
x	*Steam Quality (%)*

Acknowledgements

I would like to thank my supervisors, Magnús Þór Jónsson and Halldór Pálsson for their support both before and after I moved from Iceland to Canada. I would also like to thank Landsvirkjun for the scholarship, and for seeing potential in the project from an early stage.

I would also like to thank Sturla Birkisson, and Jardboranir hf. for allowing me to continue my studies while working, as well as providing cost figures to the project.

And finally, Hallveig Broddadóttir and my son Magnús for putting up with a tired and very distracted partner and father.

Chapter 1

Introduction

In recent years, much of the focus of geothermal research has been on enhanced geothermal systems (EGS); this is primarily due to the lack of naturally occurring hydrothermal systems available around the world. While many of these systems are artificially fractured hot dry rocks, the same approach to production could be applied to a high temperature hydrothermal system. In the study the reservoir and ambient conditions are representative of the Krafla geothermal field in northern Iceland; however, the method could be applied to any hydrothermal geothermal field.

Production methods utilizing pumps to produce geo-fluids as hot brines have allowed producers to extract more brine per well than would have been possible under natural flow. Unfortunately, current down hole pumps are limited to temperatures around 200°C and a setting depth of 457m [Sanyal, 2007]. If electric submersible pumps (ESP) could be utilized at higher temperatures and set deeper than shaft driven pumps, could additional power be extracted per well?

Downhole pumps could allow producers to use geothermal brines as single phase fluids. Using geothermal fluids as single phase liquid will result in higher brine temperatures; if the steam phase is not created; and to save the exergy lost during the creation of a secondary steam phase, and recover it in a binary power cycle. The aim of this study is to determine if the work put into operating an ESP could be recovered in the power plant in efficiency gains and the increase of available mass flow per wellbore.

In addition the closed loop systems have additional benefits not investigated in the study which include:

- A significant reduction of gaseous emissions to the atmosphere
- Reduction in waste water handling as most of it would be re-injected
- Reduction in solid waste to the lands surface and atmospheric emissions
- Minimize the impact of scaling by keeping minerals in solution
- Brines may also be treated at surface with additives
- Reduce the cost of the gathering system due to smaller pipes
- A minimal impact on scenic areas with buried pipelines

1.1 Scope of the study

The purpose of this study is to investigate the potential gains in power production by using geothermal brines in a sub-cooled state as opposed to two-phase fluids. Furthermore, a cost analysis will be performed using data and estimates from previous geothermal developments to see if the technology could be competitive with current geothermal production methods. The study will focus primarily on efficiency gains in the saturated power plants; however, some modeling of the wellbores and associated downhole pumps will be required to estimate the production rates of geo-fluid, and ultimately the power, retrievable.

Once the optimal amounts of power from conventional flashing technology and pumped binary systems have been estimated, a cost analysis comparing each technology will be performed, to determine the best technology for a series of reservoir temperatures ranging from 180°C to 360°C. The costs will be focused on the wellbores, completion costs and plant type.

1.2 Previous work

The idea of using downhole pumps to prevent flashing in the wellbore is not a new concept; it has been used extensively in low to moderate temperature fields around the world. One of the early pioneers of the idea was Magma

Energy Inc.; specifically their Magmamax plant in Imperial Valley, California USA. The Magmamax plant was first conceptualized in 1970 and brought online in 1979. It was one of the first operational binary power plants in the world [Dipippo, 2008].

Magmamax was not only one of the first binary plants; it was quite a sophisticated design. In the design philosophy section of a paper written by the plants' owners and engineering firm [Hinrichs, 1980] they stated, "because of ever escalating drilling costs, it was imperative that the energy extracted from each pound of brine be maximized." The plant utilized two binary cycles connected via recuperator. The plant's topping cycle was driven with isobutane which was heated using a massive counter-flow heat exchanger. After leaving the turbine, a recuperator was used to heat propane in a bottoming cycle. Since the Magmamax project, a great deal of research and development has gone into improving the thermal efficiency of binary power plants; recuperators and open feed heat exchangers are now common pieces of equipment in modern organic Rankine cycles.

Aside from the temperature gains associated by not flashing the brine in the wellbore, the design engineers were also mindful of the fact that a much higher amount of mass could be extracted per well if a downhole pump was used. While the downhole pumps did add some expense in terms of initial cost and maintenance, they were confident they could be run with ease and would ultimately prove cost effective. Although the downhole pumps used in the Magmamax process were initially frought with operational problems, they ran for up to two years without trouble [Dipippo, 2008].

1.2.1 Electric Submersable Pumps

In 2007 Subir Sanyal and his colleges were investigating "the practical range of net power capacity available from conventional and enhanced geothermal wells as a function of temperature and productivity index" [Sanyal, 2007]. The results of this paper show a clear advantage to the pumped binary system; however, since the author was taking a practical approach, he ended his investigation of pumped wells around 190°C, which is the current maximum working temperature of commercially available downhole pumps [Sanyal, 2007].

In recent years the Foundation for Geothermal Innovation, a group of engi-

neers, educators and business interests have been looking at the potential tied to the lack of available high temperature pumps. The foundation had a one day meeting to discuss some of the design criteria an ideal downhole pump would have, including diameter, deployment, flow rate, operation, sensors, efficiency, power, cabling, serviceability, cost and manufacturability [Foundation for Geothermal Innovation, 2009]. The group also discussed what kind of incentives would be needed to attract major downhole pump companies to research and develop such a pump. The results of the discussions were published as the Lemelson Report; in the report the pump development targets of the United States Department of Energy (USDOE) are also published for comparison sake. The relevant results from the Lemelson report and the USDOE are summarized in Table 1.1, along with the pump development targets chose for the current study.

Table 1.1: ESP development targets by Institution

ESP Performance Targets			
Parameter	Lemelson Targets	US Dept of Energy	Study Targets
Temperature	200°C to 225°C	275°C	Unlimited
Diameter	about 313mm	168mm to 269mm	168mm to 269mm
Flow Rate	min 60 l/s	80 l/s	80 l/s
Pressure	20.7 Bar	200 Bar	200 Bar
Power	560 kW	*1200 kW	560 kW
Reliability	3 years	Unknown	3 Years

* Estimated based on power.

The Lemelson targets are certainly achievable considering pumps deployable through $13\frac{3}{8}$ casing already exist and downhole pumps are being operated for up to 2 years without replacement in 200°C conditions in the oil sands of northern Alberta, Canada. Since these pumps are enduring two years of hot sandy bitumen; it seems reasonable to expect an operating life of three years pumping brine solutions. In the findings and recommendations section of the Lemelson report the authors note "While at the meeting, a temperature of 220 °C was selected as a target; most participants individually felt this target was too low for both geothermal industry needs and in creating a stretch target to inspire innovation". The report also states that high temperature pumps capable of 450°C and pumps with 1500 kW already exist; they are just not paired together [Foundation for Geothermal Innovation, 2009]. The current study chose to remove any temperature restrictions in the pump, however, the current study ends at 360°C. It was felt that an upper limit on flow of 80 L/s should be adequate for most applications; many reservoirs may experience the creation of an unwanted steam phase due to the massive drawdown at the pump suction, or in the reservoir. It was felt that 560 kW

would also be sufficient for most commercial applications, especially if smaller diameter wellbores are a secondary target for development as they were in this study. In practice, if large flow rates are anticipated a larger wellbore should be drilled to accomodate the high power pump. The target that was of arguably the greatest importance to prevent the creation of the steam phase is the discharge pressure. The study used the 200 Bar recommended by the USDOE, this gives the developer the ability to lift a significant columns of fluid out of the well and prevent flashing over a much wider range of temperatures.

Another problem geothermal producers are facing is from major companies not willing to sell the best products to the geothermal sector "major motor companies such as GE, Toshiba and Siemens have high temperature motor capacity but currently do not provide systems to the geothermal sector" [Foundation for Geothermal Innovation, 2009]. This may be a result of relatively small geothermal market, or fear of reprisal or boycott from oil customers who are hoping to sell thier natural gas to heat homes and produce electricity.

While the authors of the Lemelson reports took a conservative approach to ESP development targets, the United States department of energy set more ambitious targets for pump development. The government targets included smaller diameter installations, higher temperatures and significantly higher pressures. The higher pressure pump will allow for higher temperature resources to be exploited without flashing, or would remove the need for additional downhole pumps. Another setback facing pump developers is the physical length of the pumps. If the number of stages grows excessive, the pumps will need to be installed in sections and be partially assembled on location. This poses a problem for quality control of the pumps and ultimately costs associated with the pumps. The Lemelson report goes into discussion regarding sensors, cabling, serviceability, manufacturability, testing and other more practical matters not directly related to this study.

1.2.2 Enhanced Geothermal System Economics

A prerequisite to any major project is viability; will the money invested yield good returns? While returns can take many forms money, knowledge or both; the majority of stakeholders tend to be interested in monetary rewards. While this mentality can retard the advancement of new technology

sometimes, it is a necessary evil to ensure continued investment and to determine if the development is actually advancement at all. The aim of this study is to determine if preventing flashing is truly beneficial or just an exercise in thermal efficiency.

While much of the research is coming out of the United States, many of the development costs will be assumed to be of similar scale in Icelandic geothermal fields. While the majority of the costs should be consistent between a conventional plant and a pumped binary plant, special attention will be placed on the wellbores and completions.

Different sources have different methods of estimating what a potential well should cost [MIT, 2005], but all of the sources agree that there is a lot of variance in the data. The variance is a result of problems encountered while drilling. These can be minor problems which may only delay operations for a day or two, but some problems may also double the length of time and money required to complete the well. An earlier study [GeothermEx, 2004] proposed an empirical function to estimate drilling costs as a function of depth. The results of statistical analysis from earlier drilling projects found that depth accounts for approximately 56% of the cost variance in geothermal wellbores [GeothermEx, 2004].

In a 2005 MIT study, an event-based model using actual or direct costs associated to drilling a wellbore was created; the model was a simplified version of an earlier model created to estimate advanced drilling technique costs [MIT, 2005]. The model was called Wellcost Lite and it calculates costs per casing interval and includes time, materials, rentals, and secondary service providers such as well logging. The Wellcost Lite model estimates for various depths ranging from 1500m to 10,000m are shown in Table 1.2; the EGS wells in the study were not completed with downhole pumps or production tubing so these cost would be in addition to those figures.

Table 1.2: EGS well drilling cost estimates from Wellcost Lite.[MIT, 2005]

Shallow			Mid Range			Deep		
Depth, m	No. of Casing Strings	Cost, million $	Depth, m	No. of Casing Strings	Cost, million $	Depth, m	No. of Casing Strings	Cost, million $
1500	4	2.3	4000	4	5.2	6000	5	9.7
2500	4	3.4	5000	4	7.0	6000	6	12.3
3000	4	4.0	5000	5	8.3	7500	6	14.4
						10,000	6	20.0

Unfortunately, no such study relating borehole depth and diameter to cost was found. The large diameter intermediate casing strings and liners are standard in geothermal well designs due to the high mass flow rates; perhaps this is why no investigation into diameter was found.

The largest expenditure for a producer without a doubt is the power plant accounting for 54% on average of the total development costs [Geothermal Energy Association, 2005]. Power plant design is largely influenced by the reservoir temperature and the chemistry of the brine; some other factors could include the availability of cooling water and the ambient temperatures. Historically the lower temperature resources have been developed using binary technologies and the hotter reservoirs with a flashing system. The binary systems are usually more capital intensive than their flashing counterparts; which could be why they are often favored over binary systems in temperature ranges where either technology could be applied.

In Appendix A.1 the values estimated in previous economics studies are shown; the high end values are related to the feasibility thresholds to many of the projects and come from the price of power. Similar to the drilling, the costs associated with plants are also influenced by supply and demand; the price of materials like steel, concrete and the availability of labor and equipment can change the final cost significantly.

1.3 Objectives of the study

The first law of thermodynamics demands that the enthalpy for each kilogram of geothermal fluid remains constant as the fluid changes from a liquid to a two phase mixture. Figure 1.1 below is generated by plotting the exergy destruction per kilogram of fluid, if the fluid was taken to the ambient dead state temperature and pressure. While the saturated brine has the same enthalpy as the two-phase fluid, it will have more available exergy than its two-phase counterparts, meaning that some exergy is lost to the phase change during production. An example of a similar calculation is shown in the methods and materials section as the same calculation is used to determine the exergy destroyed during reinjection.

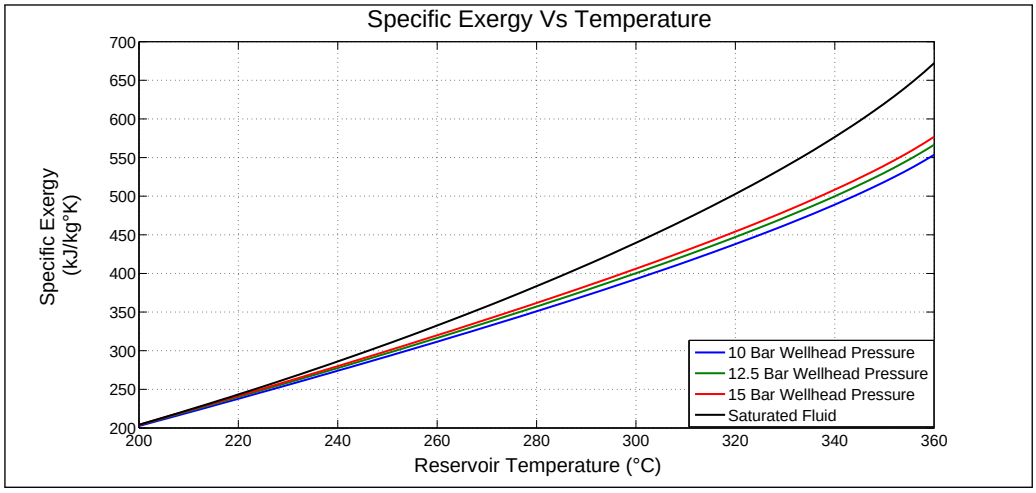

Figure 1.1: Calculated Exergy at well bottom and wellhead pressures of 10, 12.5 and 15 Bar

The two curves in Figure 1.1 could also be plotted as functions of steam quality, as they are subject to a relevant flowing wellhead pressure. As the wellhead pressure approaches the fluids saturation pressure the curves will come together. Unfortunately this would mean no production for a conventional geothermal well. In addition to the gains in available exergy, the resultant fluid will be hotter than a two phase mixture of similar enthalpy and a power cycle may be able to run more efficiently at the resulting higher temperatures.

1.4 Economic Benefits

While Icelandic geothermal developers are not in direct competition for drilling rigs with the oil and gas industry as they are in many parts of the world, they will still pay more for equipment and services when oil prices are high. The equipment and services provided by oil service companies such as drill bits, mud supplies and directional drilling services will increase with the price of oil.

The MIT Depth Dependent (MITDD) drilling-cost index [MIT, 2005] was based on thirty years of available onshore oil well drilling data collected by the American Petroleum Institute (API). After having gathered all of the cost data for different depth intervals, the index was normalized to the 1977 U.S. dollar. The trends seen in Figure 1.2 are based on the ratio to 1977 U.S. dollars and are adjusted for inflation. The small hump around the late 1970's to early 1980's reflects the costs sharply rising due to the oil crisis; the trend then levels out until another sharp increase is seen around the year 2000 which could be a response in the commodity prices due to wars in the middle east.

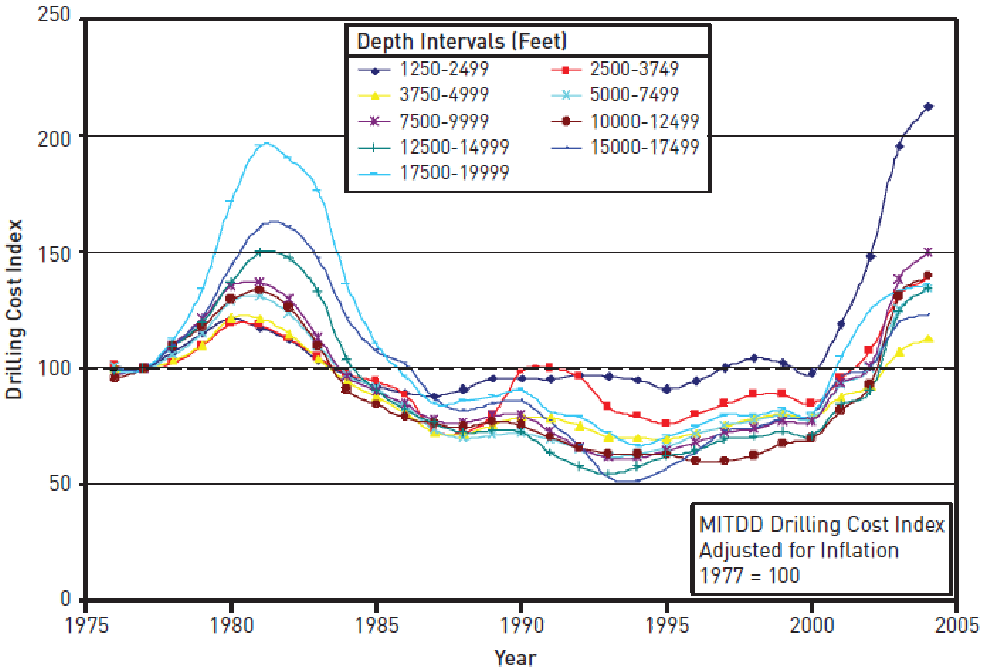

Figure 1.2: Average cost per well for each drilling depth interval adjusted for inflation.[MIT, 2005]

Another interesting conclusion which can be drawn from the drilling cost index adjusted for inflation, is that the cost to drill a well stayed below 1982 levels for nearly twenty years. The slopes of the cost index lines from 1976 to 1981 are similar in magnitude to those of 2000 to 2005; this means the costs are increasing just as fast as in past years and reducing drilling costs should be a major priority to developers.

Advances in drilling technology allow wells to be drilled faster; however, service companies often charge a premium for the new technology to help offset the development costs. An alternative way of reducing drilling costs while maintaining wellbore quality is to get more energy out of each well. If the same well could produce more energy with the aid of a downhole pump than allowing to flow under its own power, this would be a relatively cheap addition to an existing wellbore and could potentially reduce the total number of wells drilled.

Since great care is placed in making power plants as efficient as possible, trying to save money on the plant side is much more difficult since they are relatively lean to start with and many of the parts such as heat exchangers, turbines and steam separators are custom designs. The steam gathering system is another area of potential savings since a single-phase fluid would not require such large diameter flow lines. It represents a relatively small cost when looking at the total costs for field development. The drilling and completion of a fields' wellbores is often the second highest expense [Geothermal Energy Association, 2005] for producers and maximizing the net power out of each well could reduce development costs substantially.

1.5 Environmental Benefits

The environmental benefits of any geothermal power technology over coal or other forms of hydrocarbons is well documented. The reduction in carbon dioxide, sulphur dioxide and nitrous oxides has given geothermal its green technology designation. The reduction in some gas emissions does not mean that geothermal has achieved zero environmental impact; it's just better than the other hundred-year-old technologies powering the world. The aim for any project should be zero impact, or to mitigate the long term environmental impacts. In [Dipippo, 2008] the author outlines a generic list of environmental impacts for electricity generation. While not all of the impacts are related

to geothermal power generation, it gives a wider scope to consider when evaluating environmental impacts.

- Gaseous emissions to the atmosphere
- Water pollution
- Solids emmisions and waste to the lands surface.
- Noise pollution
- Land usage
- Land subsidence
- Induced seismicity
- Induced landslides
- Water usage
- Disturbance of natural hydrothermal manifestations
- Disturbance of wildlife habitat and vegetation
- Alteration of natural vistas
- Catastrophic events

Since no two geothermal projects or reservoirs are the same, each item of the list could be more or less relevant between projects. While the primary focus of environmental impacts are typically focused on measurable quantities such as emission rates, water usage or land subsidence; the intangible impacts such as the destruction of a natural wildlife habitat or natural scenery can upset people just as much.

Chapter 2

Methods and Materials

2.1 Power Plant Models

The types of plants considered in the study were single-flash, double-flash and an organic Rankine cycle both with hydrocarbon working fluids and water. Two important considerations went into the selection of the Krafla geothermal field for this study. Firstly was the availability of operational data through first person contacts who have extensive knowledge of the plant. Secondly, the condensing temperature of 45°C should be easily achievable many places in the world. Although Krafla is an older plant, it has been capable of maintaining this temperature through all seasons and it closely matches the cooling water conditions of 5 °C and 100 KPa.

The analysis of the plants was done using a nodal technique where each component in the plant is assigned an upstream and downstream node; the systems' fluid properties such as temperature, pressure, enthalpy, entropy, quality were determined at each node. This information from each point allows one to determine things such as power, mass flow rates, cooling water requirements and both first and second law plant efficiencies. The other assumptions common to all of the plant models are negligible pressure and heat loss in all pipes and vessels, in addition to the pipes the heat exchangers and condensers and turbines also had no external heat loss or gain. The efficiencies for steam turbines were assumed to be seventy percent efficient while those with organic fluids were assumed eighty percent efficient, these

numbers where initially chosen while calibrating the models and appeared in the exergy paper from Yari [Yari, 2009]. The pump efficiency for the ORC process was assumed to be ninety percent efficient, this value for pump efficiency was also used from the Yari study. The plants will be compared based on power output from the turbines as the primary objective; however the first and second law efficiencies are also recorded since improvements in these areas yield more power. All of the fluid properties used in the study came from a computer program, created by the US National Institute of Standards and Technology, called Refprop.[Refprop, 2007]

Table 2.1: Common Cycle Parameters

Parameters used in the Analysis	
Parameter	Value
Dead State Temperature	278.15°K
Dead State Pressure	100 Kpa
Heat Exchanger Pinch	5°C
Water Turbine η_T	70%
ORC Turbine η_T	90%
Pump Efficiency η_P	90%
Cooling Water Temperature	5°C
Cooling Water Discharge Temperature	40°C
Minimum Turbine Steam Quality	85%

The climate values used in the study come from a recent study,[Hanna , 2004] and show the average ambient temperature for the Krafla area in northern Iceland ranging from 3.5°C-4°C, so a temperature of 5°C was used as a safe assumption. The 5°C dead state temperature was also found for exergetic analysis done on the Husavik plant [Dipippo, 2008]. The dead state pressure is based on the proximity of the Krafla field to the ocean; a pressure of approximately 1 bar was felt to be a good estimate for coastal regions. The minimum steam quality assumption of 85% comes from previous course work and modeling of power plants [Pálsson, 2009]; the constraint appears in other publications [Yari, 2009], although not always explicitly stated, the turbine exhaust was often in the 85% to 90% range.

2.1.1 Single Flash

The first type of power plant evaluated was a single-flash style with condenser. This style of plant is common around the world, as well as in Iceland, and was chosen because the plants' operating parameters were known. The single-flash plant uses a mixture of steam and water produced from self

flowing wells; the mixture is then separated at the plant into steam and hot brine. The dry steam is sent through the turbine while the remaining water

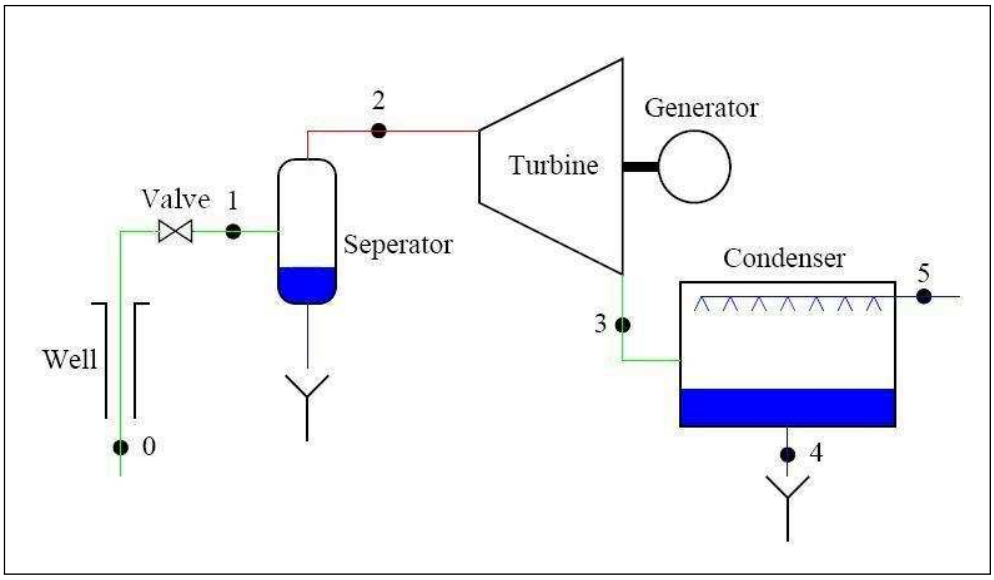

Figure 2.1: Process diagram for a single-flash power plant with condenser. [Pálsson, 2009].

The single-flash power cycle was evaluated starting from the bottom of the wellbore where brine temperature is equal to reservoir temperature and the initial quality is assumed zero; the fluid is assumed to be single-phase liquid held at saturation pressure or bubble point, this is represented by point zero in Figure 2.1. The next point occurs in the pipeline before the separator; here the fluid has been throttled through a valve so $\Delta h = 0$, however the pressure is reduced to the plants' separator pressure. At separator pressure, a secondary steam phase emerges from the liquid phase; the first law of thermodynamics demands that enthalpy remain constant so heat is removed from the liquid phase to provide the latent energy for vaporization. Equation (2.1) describes the process where the steam quality at node 1 is a function of pressure. While the phase change does not destroy any enthalpy, some exergy is destroyed in the process. The rate of exergy destruction for a throttling valve is governed by equation (2.2) where T_0 and s_0 are the properties of the fluid at the defined dead state conditions Yari [2009].

$$h_0 = h_(x_1, P_1) \tag{2.1}$$

$$\dot{E}_{DS} = T_0 \dot{m}_1 (s_1 - s_0) \tag{2.2}$$

In the plants' separator, the steam phase is separated from the geo-fluid's liquid phase; the steam is sent to the turbine while the brine is either used for a secondary purpose or discarded. The saturated steam at point two, before the turbine inlet, is assumed to be dry steam at the same temperature and pressure as the separator. The point represented by three in the diagram is after the turbine, this point is assumed to be at condenser pressure and have a quality of no less than 85%. The changes in enthalpy across points two and three yield the turbine work which is given by (2.3) with the turbine efficiency given by (2.4) where h_{3s} is the exit enthalpy based on an isentropic process. The rate of exergy destruction for the turbine was calculated using (2.5).

$$\dot{W}_T = \dot{m}_2 (h_2 - h_3) \tag{2.3}$$

$$\eta_T = \frac{h_2 - h_3}{h_2 - h_{3s}} \tag{2.4}$$

$$\dot{E}_T = T_0 \dot{m}_2 (s_3 - s_2) \tag{2.5}$$

The cooling requirements for the plant are considered to be the energy required to condense the turbine discharge, or the amount of energy absorbed by the cooling water, as they should be the same. The amount heat transferred across the condenser is represented by equation (2.6) and rate of exergy destruction by (2.7). While open heat exchangers are not common, they can be used if water scarcity is not a problem. After leaving the condensing unit the fluid is reinjected. While this has no power input or output, some potentially useful heat is discarded from the plant, meaning some exergy is destroyed. Equation (2.8) was used to calculate the exergetic destruction rate due to reinjection.

$$\dot{Q}_C = \dot{m}_3 (h_3 - h_4) = \dot{m}_5 (h_4 - h_5) \tag{2.6}$$

$$\dot{E}_C = T_0(\dot{m}_4 s_4 - \dot{m}_3 s_3 - \dot{m}_5 s_5)) \tag{2.7}$$

$$\dot{E}_R = \dot{m}_{2L}[(h_{2L} - h_0) + T_0(s_{2L} - s_0)] + \dot{m}_4[(h_4 - h_0) + T_0(s_4 - s_0)] \tag{2.8}$$

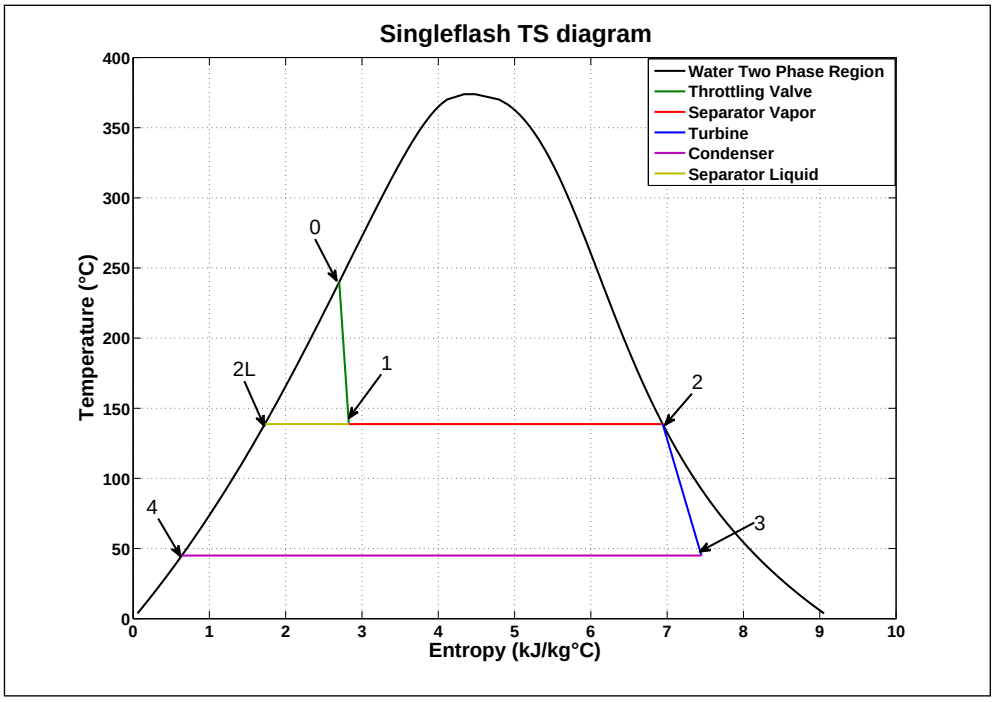

Figure 2.2: TS diagram for a single flash power plant with condenser.

The T-S diagram shown in Figure 2.2 gives a representation of the process from a thermodynamics point of view. The well bottom is represented by the point 0 which lies on the left side of the two-phase envelope representing a single-phase liquid. The point 1 in Figure 2.1 is after the throttle valve, and while enthalpy is conserved, entropy is not. This pressure drop creates entropy according to equation (2.2), which is why the line between point 0 and point 1 is not vertical.

The separator is represented by the long horizontal line, the line which starts at point 1 ends at the point 2 represents saturated vapor and the line travelling from point 1 to point 2L is saturated liquid. While the separator does

not affect the enthalpy or entropy, it does separate the two phases created after the throttling valve. The vapor phase does, however, have significantly higher enthalpy as a result of the creation of the secondary steam phase, which has the same energy as the liquid, as well as the latent heat of evaporation. The line is horizontal because boiling is an isothermal process and the turbine is using only dry steam. In the process diagram point 2 is the dry steam used by the turbine, and the line ending at point 2L is re-injected fluid.

The turbine expansion is represented by the line which goes from point 2, the saturated vapor state at the turbine entrance, to some lower steam quality due to the pressure drop across the turbine. The drop in presure causes some of the existing liquid droplets to convert to steam and subsequently lowers the turbine output temperature at point 3. Earlier the turbine was said to be 70% efficient which is why the T-S diagram has a sloped line between points 2 and 3, reflecting an increase in entropy.

The condenser is represented by the horizontal purple line across the bottom of the TS diagram labeled by points 3 and 4. Similar to the separator this line represents an isothermal process, condensation of the steam phase which occurs at some pressure and temperature. This line shows the condensation of the remaining vapor phase generated after the removal of energy by the turbine, this condensation is necessary to keep the turbine exhaust at a sub atmospheric pressure, which yields large efficiency gains. The fluid, which is reinjected at point 4, is a liquid.

2.1.2 Double Flash

The double-flash cycle was the second type of flashing plant used as a basis for comparison. It is known to give higher efficiencies by flashing the liquid from the first separator that is discarded in the single flash process. The flashed liquid stream is then recombined with the exhaust from the first turbine and run through a second lower pressure turbine. The figure 2.3 shows a visual representation of the process, after the second turbine the liquid is condensed and re-injected or discarded.

Similar to the single-flash case in many aspects, the double flash uses all the same equations used in the single-flash case, with the addition of a an energy balance equation to calculate the enthalpy of the recombined fluid going into

the low pressure turbine. The same nodal analysis process was used to study this case, taking each components' up and downstream nodes and computing the changes in enthalpy and entropy in the working fluid.

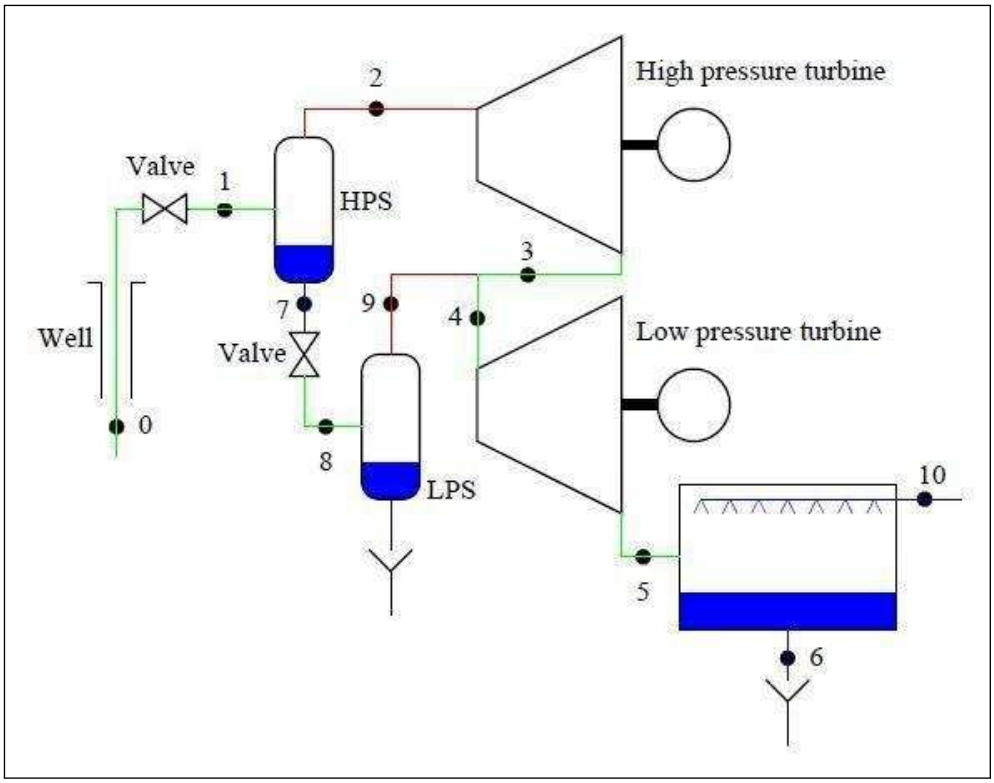

Figure 2.3: Process diagram for a double-flash power plant. [Pálsson, 2009].

The T-S diagram for the double-flash process is shown in Figure 2.4; the diagram illustrates the changes in the fluids' properties throughout the process. The geo-fluid starts as a 240°C saturated liquid and is flashed down the line, connecting points 0 and 1 to the first horizontal line representing the high pressure separator. The high pressure turbine is described by the line between points 2 and 3. The higher pressure turbine exhaust is then combined with the vapor stream from the low pressure separator (denoted by the line between points 9 and 4) and becomes the inlet for the low pressure turbine. This turbine is illustrated by the line between points 4 and 5. Similar to the single-flash case there are two liquid outlets from the separators the lines between points 1 and 7 and points 9 and 9L which represent the high and low pressure separators respectively. The high pressure liquid outlet is flashed

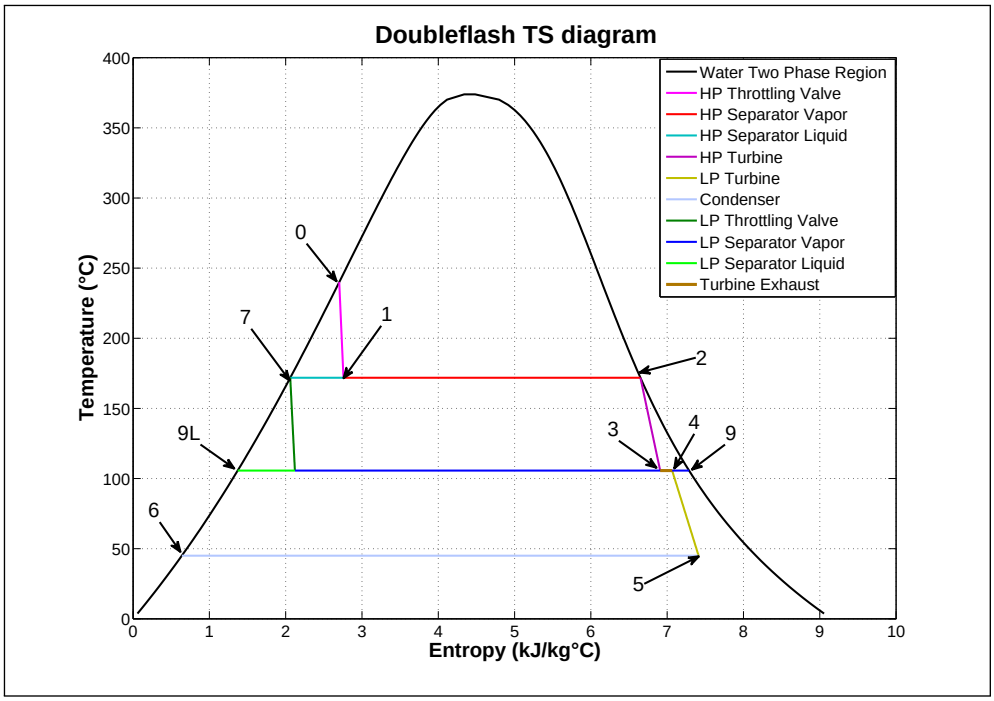

Figure 2.4: TS diagram for a double-flash power plant.

along the line connecting points 7 and 9. This represents the pressure drop across the valve between the two separators. While the temperature is lowered, the quality of the working fluid is increased as the fluid moves from the saturated liquid curve to a position in the two-phase region. The condenser is portrayed by the horizontal line between points 5 and 6 at the bottom of the T-S diagram. This process is condensation at a constant temperature; the fluid at point 6 is then reinjected or discarded.

2.1.3 ORC with Recuperator

The organic Rankine cycle or ORC has two major differences over the single and double-flash plants; the first being the working fluid is in a closed loop, the second being the working fluid is usually a hydrocarbon hence the name organic. The closed loop design has a few major benefits, the first being there is no need for a large gas extraction unit, which is a heavy power consumer. Some operational benefits of using a hydrocarbon working fluid over water are a mitigated threat of scaling and corrosion in the turbine and condenser. The hydrocarbon fluids can be tailored to a specific temperature range to

maximize the power output. H. Pálsson stated most organic working fluids also have desirable properties regarding retrograde condensation (personal communication, July 2011). Retrograde condensation occurs after a pressure drop such as a turbine, many organic fluids will travel from a saturated steam into the supercritical region and back to the saturated steam point. This property allows larger amounts of energy to be removed before encountering a quality constraint. If on Figure 2.6 for example, a line was drawn from the saturated vapor curve for isopentane straight down, it will not encounter the saturated line again until a substantial change in temperature has occured. Water, however, will immediately begin to condense in the turbine until the quality constraint is reached.

The model was capable of calculating the cycle's properties in three possible scenarios, two being the fluid is below supercritical pressure, meaning the fluid leaves the boiler as a saturated steam, or a steam heated past the saturation point into the supercritical region. The process of heating steam beyond saturation is common in coal fire power plants, while using saturated steam is common in geothermal power generation. The other possible cycle exists over the supercritical pressure meaning the fluid passes directly from a heated compressed liquid to a super saturated steam without a two phase mixture ever present. The figure 2.6 shows an example with isopentane and a reservoir temperature of 240 °C; in the example the solver found the supercritical solution to be optimal.

The ORC has been studied and improved by many different people over the years; the additions of recuperators and open feed organic heat exchangers (OFOH) have increased the efficiency of this process further. The cycle with a recuperator was used in the study because the OFOH configurations did not always yield more power, but occasionally obtain higher thermal efficiencies by bleeding a stream from the early turbine stages and recombining it with the stream after the pump. The study by Yari [2009] compared various configurations of geothermal power plants and concluded that the addition of many of these OFOH and recuperators did not outperform even a simple ORC in terms of thermal efficiency or net work obtained. While these additions often make the cycle more efficient, the energy saved by the OFOH is often lost somewhere else, which is why the power output is similar. A process diagram of the ORC plant used in the study is shown in Figure 2.5.

Equations (2.9) and (2.10) describe how the power and exergy destruction rates were calculated for the cycles containing heat exchangers. The exergy destruction can also be visually compared by looking at the gaps between

the two fluids temperature profiles in Figure 2.7, large areas between the temperature profiles indicate poor second law efficiencies.

$$\dot{Q}_{IHE} = \dot{m}_2(h_3 - h_2) = \dot{m}_6(h_6 - h_7) \tag{2.9}$$

$$\dot{E}_{IHE} = T_0(\dot{m}_2(s_3 - s_2) + \dot{m}_6(s_7 - s_6)) \tag{2.10}$$

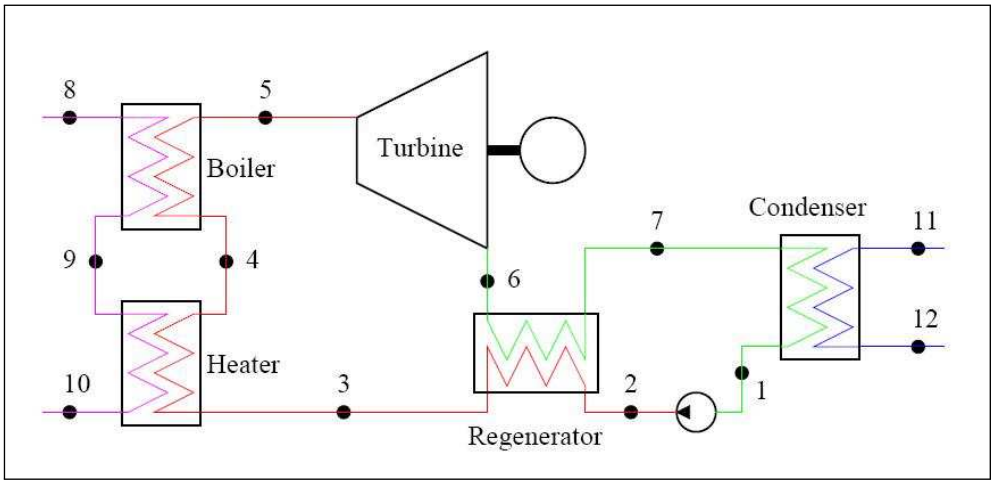

Figure 2.5: Process diagram for an ORC plant with recuperator. [Pálsson, 2009].

The closed loop approach to power generation and the addition of three heat exchangers to the process does add some complication. The process of exchanging heat between different fluids with different heat capacities and phase changes creates the potential for pinch points in the heat exchangers. A pinch point is a place where the fluid on the cold side approaches a similar temperature to the fluid on the heat exchangers hot side. These can occur anywhere in the heat exchanger, but are common around a phase changes since the rates of heat transfer abruptly change on either the hot or cold side. A pinch tolerance of 5°C was used to model all heat exchangers to ensure a minimum temperature differential of 5°C between the hot and cold fluids was maintained at every point.

The T-S diagram for the ORC shown in Figure 2.6 has some very noticeable differences over the previous cycles, mainly, that the process takes place

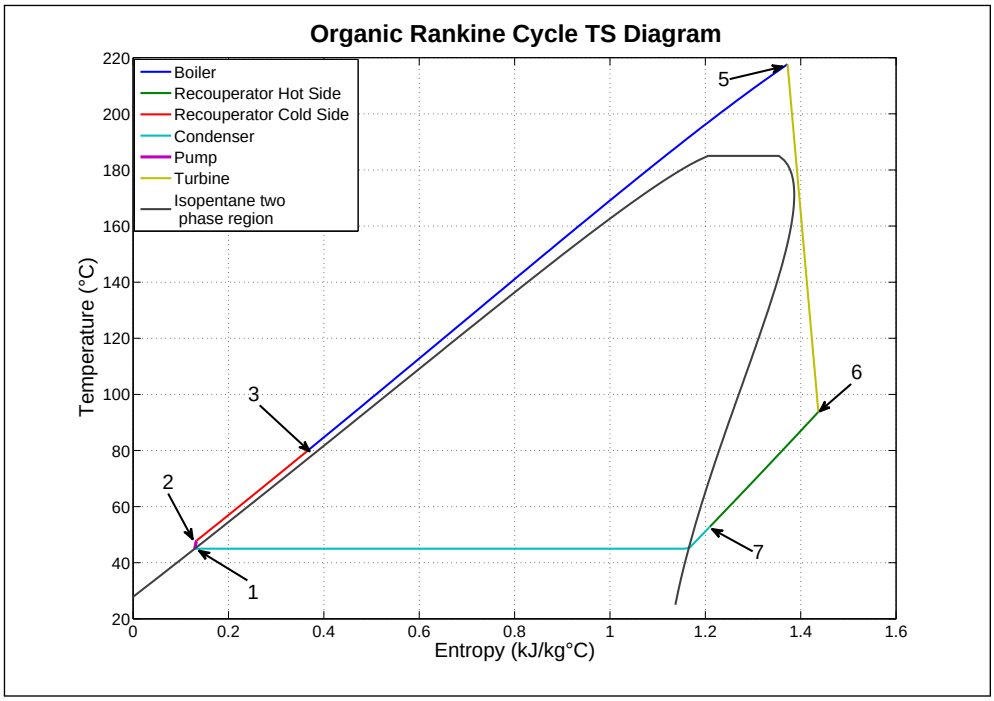

Figure 2.6: TS diagram for an organic Rankine power plant.

around the two-phase region shown in the diagram as the black curve. Other differences include the lack of separation processes which simplify the diagram and allow the viewer to look almost exclusively at the power cycle. The fluid is superheated in the boiler, represented by the line between points 3 and 5, traveling parallel to the saturated liquid curve, and continuing past the critical point. The turbine is portrayed by the line ending at points 5 and 6, traveling from the peak of the boiler curve to the recuperator curve between points 6 and 7. The turbine was constrained from entering the two-phase region by a retrograde condensation constraint. The line joining points 7 and 1 represents the condenser which is cooling more than in the flashing cycles. Notice the line starts in the superheated region; this means cooling, then condensing, which is also seen in the condenser section of Figure 2.7. The condensing line continues until the saturated liquid line where it meets a small vertical line between points 1 and 2; the vertical line describes the effect of the cycles' pump on the working fluid.

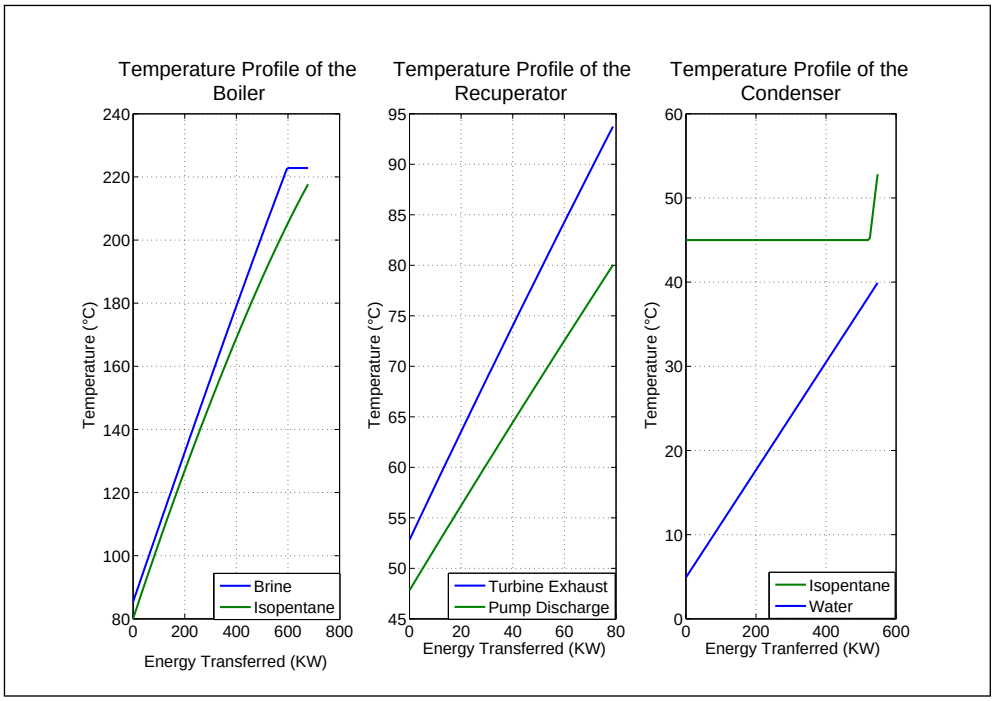

Figure 2.7: Heat Exchanger Pinch Analysis

2.1.4 ORC with Water

The ORC with water as a working fluid was proposed as a result of the common usage of water in coal and nuclear power plants. Water was also investigated to see if the performance would suffer greatly by using this safe, abundant and cheap working fluid. Water does have a lot of advantages when thermodynamics, safety and the environment are considered. Water has some very desirable thermodynamic properties such as a high specific heat capacity, higher density than most organic working fluids and high heats of vaporization. The safety issue using coal fire boilers with organic fluids means a leak in the pipe could spell disaster and many of these organic fluids are carcinogens which are dangerous to the workers and difficult to dispose of after the plants' life.

Figure 2.8 shows a process diagram similar to the ORC with organic fluids, except the recuperator has been removed. The recuperator could not maintain the heat exchanger pinch constraints without greatly reducing the power output from the cycle. In a water-driven cycle the water leaves the turbine as a two-phase mixture, not a superheated vapor. While there is a

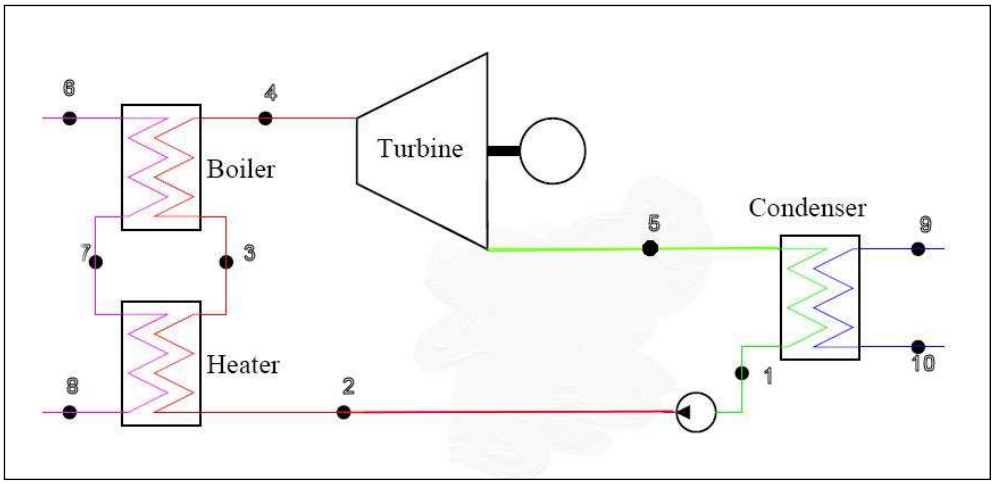

Figure 2.8: Process diagram for a simple ORC plant. Adapted from [Pálsson, 2009]

benefit to removing heat from superheated vapor, there is no benefit using the recuperator as a condenser.
The heat exchangers shown in Figure 2.9, portray a very large area in between the hot and cold sides of the plants boiler, this is a sign that a lot of exergy is being distroyed in the heat transfer process [A.Schuster et al., 2010]. Ideally, the area between the hot and cold sides of a heat exchanger should minimized to ensure the least amount of exergy is distroyed across the boiler. Comparing the exergy distruction rates in the boilers of this model with the previous cycle using a supercritical organic fluid can be done visually. In Figure 2.9 the lines appear to have two large triangles of area, while, Figure 2.7 has only a thin strip. This may be one of the reasons why this cycle performed so poorly.

The T-S diagram for the water-driven ORC shown in Figure 2.10 has taken a route similar to those used in coal fire plants, staying below the critical point, and superheating the resulting vapor. This has two distinct thermodynamic advantages. A larger change in enthalpy yields more power, also the super heating increases the entropy and helps with the quality constraint. The argument might be made that an increase in mass flow could yield similar power from the same amount of brine. However, this could require upscaling the plant for higher mass flows. In Figure 2.10 the boiler is represented by the line which extends from the saturated liquid at point 3, past the saturated vapor line over into the superheated region ending at point 4. The turbine is

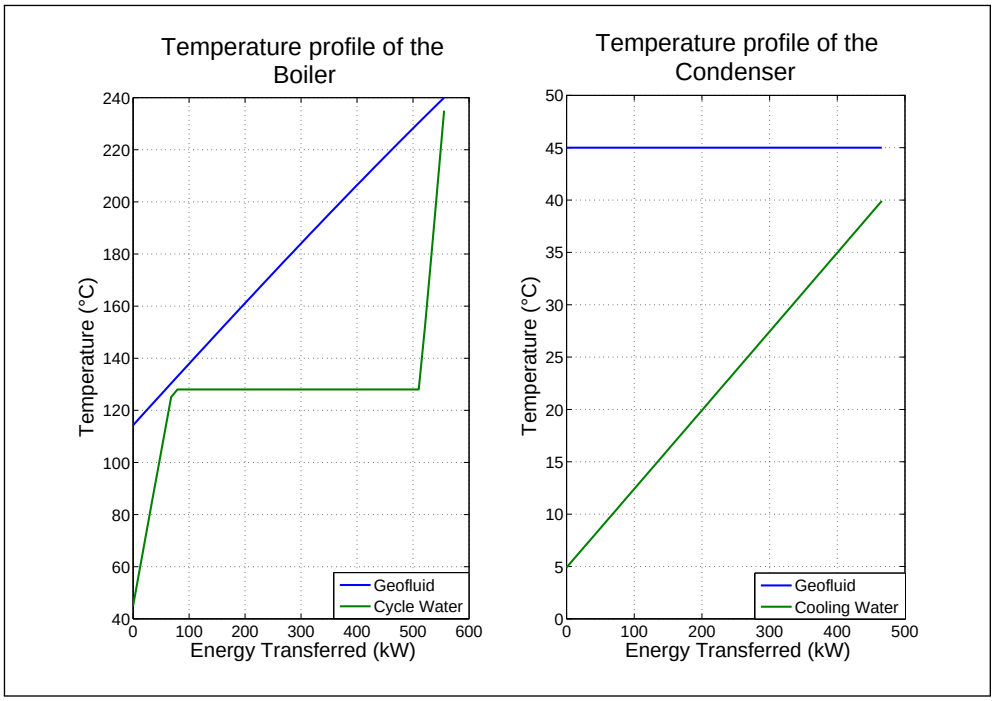

Figure 2.9: The heat exchangers in the ORC with Water

represented by the line connecting points 4 and 5, it travels from the boiler exit down to a two-phase mixture at some quality. The parallel line running across the bottom of the diagram between points 5 and 1 from the turbine to the saturated liquid line is the condenser. The pump is represented by the very small line between points 1 and 2 which is very small since little work is performed on the fluid in this cycle, however, it connects the condenser to the boiler as depicted in the process diagram. It should also be noted that this diagram is the solution for the case of the 240 °C geothermal brine. At lower temperatures, this was not an optimal configuration and the superheated solution would likely dominate the higher temperatures seen in coal and nuclear powerplants.

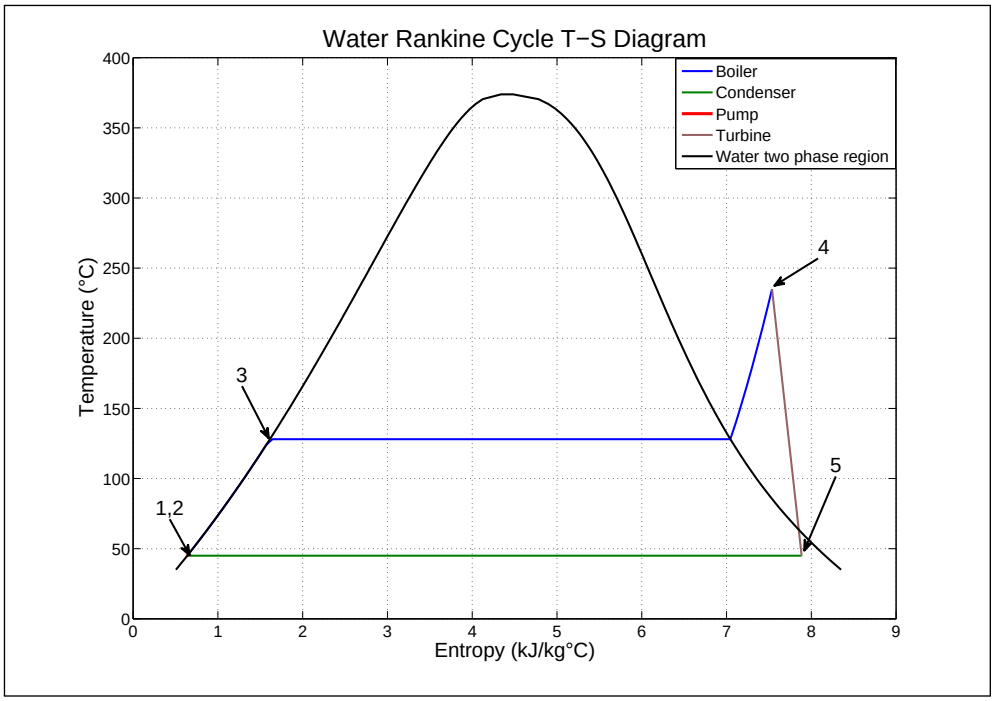

Figure 2.10: T-S Diagram for the ORC with Water

2.2 Wellbore Modelling

The wellbore modeling is largely based on a nodal analysis technique, meaning the flow path from reservoir to power plant will be broken down into sections and evaluated piece by piece. The first portion of this process will involve taking the geothermal fluids from some point in the reservoir (node 1) to the bottom of the wellbore (node 2), as seen in Figure 2.11. The aim of the model is to estimate a steady state flowing bottom hole pressure at a specified mass flow rate.

Considering the wellhead as node three, the tubing and casing design can be optimized for either cost, work or a combination of both. The pipeline design from wellhead to plant separator or heat exchanger could be optimized as well in practice, but will be ignored for this project for both time constraints and relevance to the scope of the project.

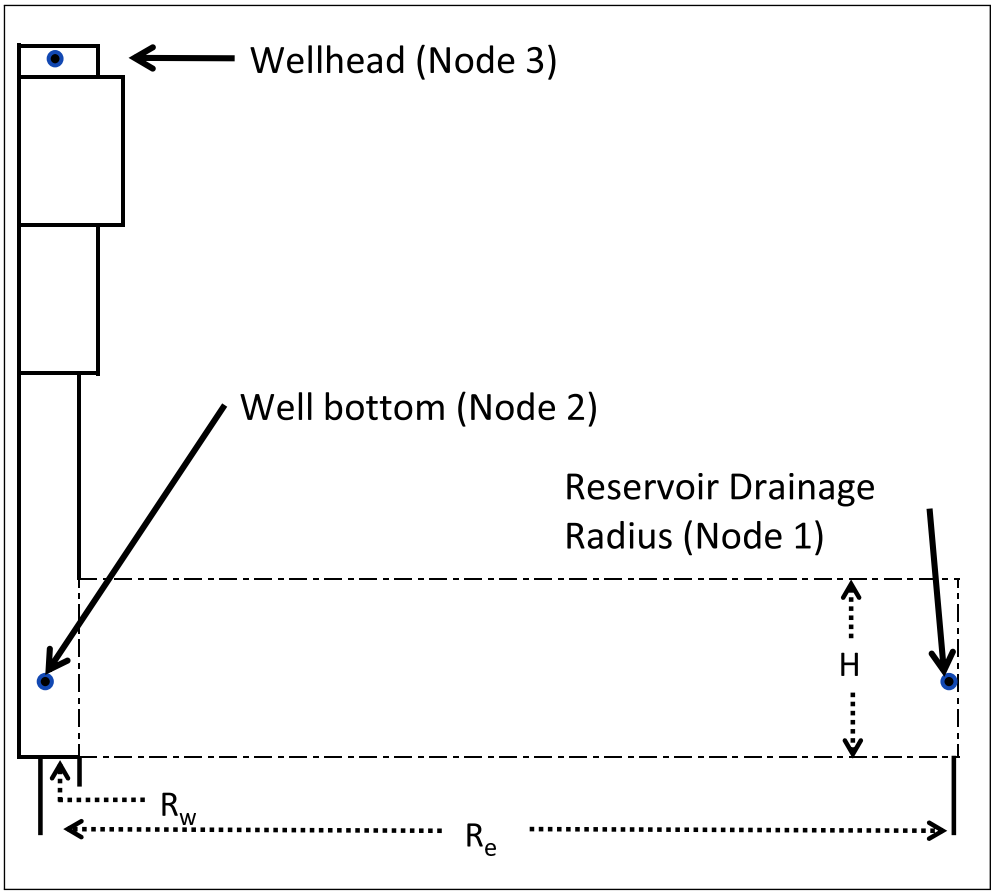

Figure 2.11: A visual representation of the 2-D reservoir model.

2.2.1 Reservoir Model

The reservoir was not a main focus in the study; however, a simple model was constructed to allow an estimation of the initial pump setting depth. The problem is that once a reservoir starts production, the water level surrounding the wellbore begins to fall; the aim of this model was to determine a safe depth to prevent pump cavitation and flashing of the geo-fluid. The model did incorporate some known physical properties of the Krafla geothermal field; the properties listed in Table 2.2 were used to estimate the subsurface fluid-flow. While multiple sources were investigated for the reservoir properties of Krafla, the majority of the information came from Bodvarsson [1989] with the remainder coming from the work of Dr. Gudni Axelsson [Axelsson, 2009] and Khalilabad [2008].

Table 2.2: Reservoir Characteristics

Parameters used in the Wellbore Solutions		
Parameter	Suggested Range	Value Used
Formation Permeability (md)	2-10	5
Permeability Thickness (Dm)	1-3	2.55
Hydrothermal System Permeability (md)	1-100	100
Porosity (%)	3-5	4
Reservoir Temperature (°C)	300-350	300
Total Dissolved Solids (ppm)	8000	0
Non Condensible Gases (%mass)	1-5	0
Formation Compressibility (Pa^{-1})	$3 * 10^{-11}$	$3 * 10^{-11}$
Water Compressibility (Pa^{-1})	$4.4 * 10^{-10}$	$4.4 * 10^{-10}$

The model first derived by Van Everdingen and Hurst [Towler, 2002], assumed that the production was constant and flowing pressure would decrease in the wellbore then eventually level out due to the constant boundary pressure effects on the solution. The solution initially acts as an infinite reservoir until the transient pressure wave makes contact with the reservoir boundary, after which the solution experiences the boundary effects. The constant pressure was assumed to simulate either injection wells or the presence of an aquifer at some distance.

$$r_{eD} \equiv \frac{r_e}{r_w} \tag{2.11}$$

The dimensionless radius, equation (2.11) is the ratio of the assumed drainage radius to the wellbore radius, where r_e is the reservoir drainage radius and r_w refers to the wellbore radius. The solution requires a boundary condition $p(r_e, t) = p_i$ at $r = r_e$ and an initial condition such that $p_i = 0$ at all r and t. This means when time $t$is set to zero all of the pressure is assumed to at boundary pressure or original reservoir pressure. It is counter-intuitive to set initial reservoir pressure to zero, however, once the dimensionless terms are converted to actual pressure values the solution makes sense.

$$P_D \equiv \frac{2\pi kH(p_i - p)}{q\mu} \tag{2.12}$$

The dimensionless pressure term (2.12) contains the Darcian flow variables for radial 2-D flow. The term requires permeability k in (m^2), H represents the height of the production interval (m). Flow rate is decipted as q, with

units of (m^3/s) and μ is used to symbolize water viscosity with the SI units of $(Pa \cdot s)$; the pressure terms portrayed by P_i and P are measured in (Pa).

The solution for the bottom hole flowing wellbore pressure as a function of time described by Van Everdingen and Hurst, takes the steady state solution represented by the $ln\ r_{eD}$ and adds the transient Bessel terms. At longer times, when $t_{Dw} > \frac{1}{4}r_{eD}^2$ the transient Bessel terms approach zero, and the steady state term can be used to approximate the solution. Since interest is only in where the final water level will be, only the steady state solution will be considered.

$$P \equiv P_i - \frac{ln(r_{eD})q\mu}{2\pi kH} \tag{2.13}$$

The steady state form of the equation used to estimate the flowing bottom hole pressures is represented by equation (2.13). The equation yields a linear pressure drop as a function of flow rate, since dissolved gasses were not considered in the model. This simple model does not account for skin factor or turbulence in the formation, it provided a starting point for wellbore modeling purposes.

2.2.2 Two-Phase Wellbore Models

The method described in the reservoir section provided an estimation of the flowing pressure at the bottom of the wellbore given some constant boundary pressure at a radial distance from the center of the wellbore. The next step in the nodal analysis will involve moving the fluids from the bottom of the well to the wellhead at some constant flow rate. The flowing wellhead pressure is a function of mass flow, depth, pipe diameter and the properties of the fluid being transported.

The project will have two types of wellbore configurations. The first a conventional large diameter wellbore with a slotted liner hung from a intermediate casing string set at 1000 meters. The second, will have a downhole pump hung from a string of production tubing. Other considerations include using the same number of casing strings which will be set at the same depths. The casing depths may be a product of geological constraints and it simplifies the comparison to keep them the same. A graphical representation of the two types of wellbores is shown in Figure 2.12.

Although the conventional wellbore is a proven technology, estimating a wellbores' potential prior to well testing is not an exact science. The challenge of estimating a wellbore pressure profile is minimizing errors in flowing bottomhole pressure in addition to single and two-phase wellbore flow. While it is generally accepted that the single phase pressure loss equations for Newtonian fluids in pipes is relatively accurate, the two-phase measurements are far from perfect, with many of the commonly used correlations are still between 20% to 100% error. The two-phase model used in the project was the Friedel correction factor, it was selected for its simplicity and relatively low amount of error compared to the other models. The model is based upon the single-phase fluid pressure drop would be for a given length of pipe, afterward, it's multiplied by a two phase scaling factor to estimate the two phase pressure drop for that given length of pipe.

The single-phase pressure drop for a liquid was calculated using Equation (2.14), the acceleration term was dropped, as it is normally a relatively small number. The two remaining terms are the dominant terms in wellbore flow, hydrostatics and friction. In single-phase flow the hydrostatic term is typically the larger of the two contributors to pressure drop. In the single-phase case, ρ represents the fluids density, θ is the inclination of the wellbore from vertical, and g_c is the gravitational constant. The friction term includes the

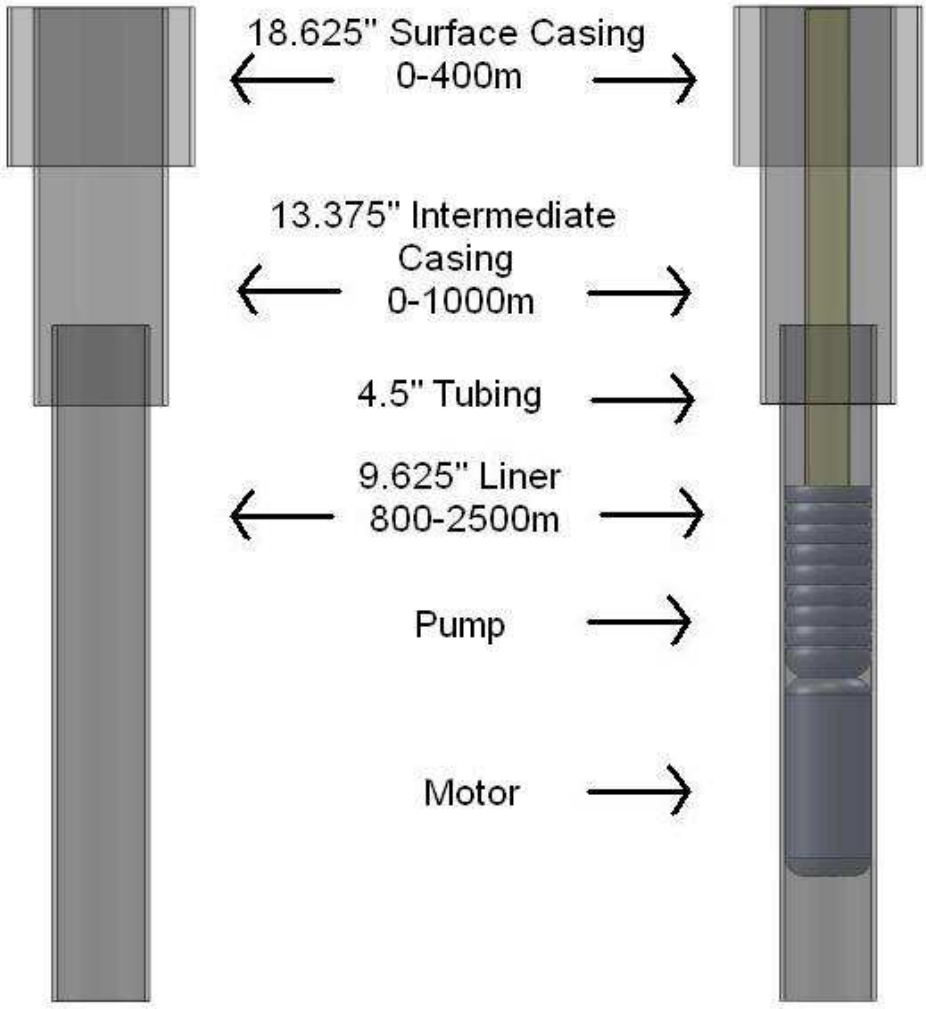

Figure 2.12: The two proposed wellbore configurations considered for the project

friction factor portrayed by f, the fluids' velocity represented by v and the pipes' inner diameter as letter D. In the hydrostatic term, the fraction $\frac{g}{g_c}$ appears as a result of the per unit length pressure drop. In practice the wells' inclination and change in measured depth will determine the change in vertical depth. The Bernoulli equation often has $sin\theta$ in the hydrostatic term, however, since drilling engineers are usually speaking in terms of vertical depth, the convention of taking the angle from vertical has been adopted in industry, and thus, $cos\theta$ is used.

$$\frac{dp}{dL} = \frac{g}{g_c}\rho\cos\theta + \frac{f\rho v^2}{2g_c D} + \frac{\rho v dv}{g_c dL} \tag{2.14}$$

The single phase pressure drop equation gives us the $\Delta p_f^{Single\ \ Phase}$ term used in Equation (2.15). This term will be multiplied by the correction factor.

$$\Delta p_f^{Two\ \ Phase} = \Phi^2 \Delta p_f^{Single\ \ Phase} \tag{2.15}$$

Where the Friedel correction factor in this case is represented by the Φ^2, a more detailed explanation of the correction factor is provided below.

$$\Phi^2 = E \ \ + \frac{3.24 * FH}{Fr^{0.045} We^{0.035}} \tag{2.16}$$

The dimensionless Froude and Weber numbers are used in the development of the correction factor. The model also declares a few new variables to tidy up the representation of the equation; these are the letters E, F and H. The letters and dimensionless numbers will be shown below as well as details to the application in the project.

$$E = (1 - x^2) + x^2 \frac{\rho_l}{\rho_g} \frac{f_g}{f_l} \tag{2.17}$$

In Equation (2.17) x represents steam quality, ρ_g and ρ_l are the gas and liquid phase densities. Finally, f_g and f_l are single phase friction factors, meaning the friction factors as if only gas or liquid was present in the pipe.

$$F = x^{0.78}(1 - x^2)^{0.24} \tag{2.18}$$

$$H = \left(\frac{\rho_l}{\rho_g}\right)^{0.91} \left(\frac{v_g}{v_l}\right)^{0.19} \left(1 - \frac{\rho_g}{\rho_l}\right)^{0.7} \tag{2.19}$$

In Equation (2.19) two additional values v_g and v_l, are the gas and liquid velocities respectively. These are needed to incorporate a slip velocity. In the project, Moody's equation was used to estimate the liquid and gas velocities, shown in Equation (2.20).

$$S = \left(\frac{\rho_l}{\rho_g}\right)^{\frac{1}{3}} \tag{2.20}$$

$$Fr = \left(\frac{\dot{m}}{A}\right)^2 \frac{1}{g_c D \rho_m^2} \tag{2.21}$$

In the Froude number calculation, a mass flow represented by $\dot{m}$ is divided by the cross sectional area represented by A. The other constants in the equation are the gravitational constant g and pipe diameter D. The ρ_m is the average mixture density calculated by Equation (2.22).

$$\rho_m = \frac{1}{\frac{x}{\rho_g} + \frac{1-x}{\rho_l}} \tag{2.22}$$

$$We = \left(\frac{\dot{m}}{A}\right)^2 \frac{D}{\sigma \rho_m^2} \tag{2.23}$$

The Weber number did require one additional piece of information that the other constants did not. This was a value for the surface tension of the liquid phase. Fortunately, Eötvös [PHYWE , 1998(@] provided a simple to-implement rule to estimate the surface tension of water up to its critical point. The rule is shown below.

$$\sigma V^{\frac{2}{3}} = k(T_c - T) \tag{2.24}$$

When using water with Equation (2.24) the molar volume V is about 18ml/mol while the constant k is about $2.1 * 10^-7\ JK^{-1}mol^{-2/3}$ and T_c is the critical temperature of water.

The result of all the pressure drop modeling is the prediction of the flowing wellhead pressure at various flow rates. The wellhead pressure is useful to determine the maximum amount of fluid can be produced before the pressure drops to unacceptably low levels for use in a single or double-flash power cycles. In the study, the plants required at least the optimal separator pressures to be produced from the wellhead. In practice it would have some tolerance for pipeline pressure losses. The lower pressure limit allowed an upper limit of mass flow per well to be estimated. The upper limit on mass flow, along with the optimized power plant calculations from the earlier sections, provide an estimate for the power per well.

2.2.3 Pumped Wellbore Models

The downhole pump requirements, like the power plants, are critical to the project. If the method cannot create more power than it requires, it will be a tough sell to plant owners. The model described below has two parts. The first is an algorithm to determine where the pump should be set, the second half determines the power requirements and plots a profile showing the pressure as a function of depth.

The pump setting depth was determined using the flowing bottom hole pressure obtained from the reservoir modeling, assuming a given volumetric flow rate. Starting from the flowing bottom hole pressure, a pressure gradient for the wellbore was constructed using equation (2.14) [Beggs, 2003]. The pressure profile was used to determine the dynamic boiling depth at a given flow rate. The pump was set 100 meters below the calculated flowing boiling depth to prevent cavitation at the pump suction. It should also be noted that the flowing pressure drop in the determination of the pump setting depth is being calculated in the wells' production liner or intermediate casing string. The pump power requirements were calculated using the pressure drop equation in the production tubing which the ESP will hang from and pump through.

Since the purpose of the pumps is to prevent boiling in the wellbore, a safety factor of 2 Bar was kept over the boiling pressure on the Electronic Submersible Pump (ESP) discharge tubing. The pump work for the ESP was determined using Equation (2.25); the solver supplies the algorithm with values for discharge pressure and flow rate in an attempt to maximize the power output from the system. Pump efficiency was assumed to be constant for all

temperatures and contains an overall efficiency including the motor, shaft, and pump.

$$W_{pump} = \frac{(P_{Discharge} - P_{Suction}) * Q_{Water}}{\eta_{pump}} \tag{2.25}$$

The consumption was then subtracted from the power the plant could generate from the brine being pumped. The model was then run with several different sizes of production tubing, to determine how power output would change with tubing diameter and, indirectly, wellbore diameter.

2.2.4 Economics Model

Initially, the economics model for the project was going to include all costs ranging from transmission lines to operational costs. The grand scale comparison fell apart because of the massive variation in power development costs recorded and estimated from various authors over the years. The table entitled "Capital cost of geothermal power technologies" in Appendix A shows some of the figures previously published. In an effort to keep the comparison fairly transparent, the economic models were simplified to the absolute simplest form to make the comparison as direct and relevant as possible.

Intuitively it's easy to imagine that the exploration, transmission, administration and costs based on the reservoir should be similar regardless of the technology used, so the comparison could just as well be made without these expenditures. The costs remaining to be compared are those of the wellbores and the power plants, which usually accounts for approximately three quarters of total development costs [Geothermal Energy Association, 2005]. While it's generally accepted that binary plants are more expensive than flashing technology, a large area of overlap is seen in the cost figures between double-flash and binary development costs. In addition to the installation costs overlapping, the maintenance costs associated with single-phase fluids are reported lower than their multiphase counterparts in both the plants and wellbores. If those assumptions are accurate, it might be reasonable to assume that savings in initial installation costs would be lost to higher maintenance costs later. In any event, the total costs associated with the plants should be about fifty percent [Geothermal Energy Association, 2005].

As a result of the simplifications, we are left comparing wellbores with three

different types of power cycles. And to mitigate the differences in wellbore costs, which are also highly variable, a base case comparison was chosen. The approach was also used because of the lack of available data comparing wellbore costs to diameter. Even if some material costs could be accurately estimated, the time required to drill these wells would be difficult to estimate.

The only source of cost variability left in the economic comparison is the downhole pump and the production tubing. The prices for production tubing and casing was gathered from two sources: Alberta Tubular in Calgary, Alberta, Canada and Jardboranir HF in Kopavogur, Iceland. While Jardboranir did not have the prices for tubing, the figures gathered from the casing costs were used to estimate what Jardboranir would likely pay for tubing based on the Alberta prices. A trend was seen when comparing the 177.8mm, 244.5mm and 339.73mm casings from Iceland to the prices provided by Alberta Tubular. The trend showed that the Jardboranir tubing prices were 68% of the Alberta Tubular's book prices for the 177.8mm and 244.5mm casings and 60% when compared to the 339.73mm casing. This combined with the wellbore model gave a basis on which to estimate the tubing prices for each temperature and mass flow rate.

The cost estimate for the downhole pump was taken from the work done by the "Lemelson Report" [Foundation for Geothermal Innovation, 2009]. The report estimated the pump would cost roughly three quarters of a million U.S. dollars. In the study, the pump cost estimate was assumed to include cabling, installation and perhaps a variable frequency drive; although these costs could be in addition to the 750,000 USD. The pump and tubing were also assumed to be replaced every three years. No workover rig costs for either model were assumed since the demands of the workover can vary significantly depending on corrosion rates and scaling.

The final component of the model took the optimal mass flows for each production tubing size and temperature range and paired it to the optimal power output for each type of cycle at that temperature. The total costs of both wellbores were then compared to the power being produced or net power in the case of the pumped well. This allowed for some performance indicators to be calculated and provided a comparison based on both installation costs and a thirty year net present value.

Chapter 3

Results

3.1 Power Plant Results

In addition to tracking the net work and exergy values for each cycle, the first and second law efficiencies were also being recorded in an effort to determine where in the cycle the power was being lost. In the following tables the specific work is represented by the letter W and specific exergy destruction is represented by E_d. The values represented by η_{nn} are different efficiency measurements; the first subscript number represents first or second law efficiency, while the second subscript number determines if it is overall cycle efficiency or based upon the energy actually taken by the cycle. In the case of the flash cycles, η_{11} would be the first law efficiency based upon all of the energy entering the plant, while η_{12} would be first law efficiency based on the power produced from the energy entering minus the energy being reinjected. The same type of analysis was done for the second law efficiency, taking the wellbore fluids entering and exiting the plant down to a dead state condition and determining how much useful work was gained for the exergy destroyed.

The results in the following tables were calculated using the models presented in the previous section, the models output was then returned to a meta-heuristic solver or Matlabs' fminbnd function in the case of the single-flash plant. The fminbnd function in Matlab uses a golden-section coupled with a quadratic search [Matlab, 7.7.0]; the algorithm was very efficient optimizing a single variable functions such as a single flash power plant. The solver

used for the remaining portions of the study uses a form of genetic algorithm called differential evolution (DE). The DE algorithm used in the study was combined with a line search method, making the algorithm incredibly robust and repeatable [Storn, 1995]. The solver also had the advantage of being easily adaptable since only the functions handle and temperature needed to be changed between trials.

Table 3.1: Single Flash Results

Cycle	Reservoir Temperature (°C)									
Parameter	180	200	220	240	260	280	300	320	340	360
W(KJ/Kg)	38.17	50.13	63.88	79.59	97.49	117.96	141.62	169.52	203.87	251.79
E_d(KJ/Kg)	110.28	131.08	153.21	176.69	201.57	228.01	256.24	286.75	320.59	361.27
η_{11}(%)	5.14	6.03	6.93	7.83	8.75	9.70	10.70	11.76	12.96	14.47
η_{12}(%)	10.43	11.60	12.72	13.79	14.82	15.83	16.84	17.86	18.94	20.21
η_{21}(%)	22.70	24.56	26.25	27.82	29.31	30.76	32.21	33.71	35.36	37.45
η_{22}(%)	41.52	43.63	45.44	47.02	48.41	49.66	50.81	51.89	52.95	54.10
P_{sep} (KPa)	141.4	193.2	260.8	348.6	462.9	613.0	813.2	1088.3	1409.4	2185.7

Table 3.2: Double Flash Results

Cycle	Reservoir Temperature (°C)									
Parameter	180	200	220	240	260	280	300	320	340	360
W(KJ/Kg)	49.38	64.55	81.86	101.45	123.59	148.69	177.39	210.87	251.58	303.69
E_d(KJ/Kg)	118.72	139.56	161.51	184.63	209.00	234.79	262.28	291.98	324.96	368.63
η_{11}(%)	6.66	7.77	8.87	9.98	11.1	12.23	13.40	14.63	15.99	17.45
η_{12}(%)	10.72	11.96	13.14	14.28	15.39	16.47	17.55	18.64	19.80	19.94
η_{21}(%)	29.38	31.63	33.63	35.46	37.16	38.77	40.35	41.94	43.64	45.17
η_{22}(%)	42.33	44.56	46.49	48.17	49.67	51.02	52.27	53.46	54.62	54.85
HP_{sep} (KPa)	290.2	419.4	593.5	825.5	1132.9	1539.7	2082.9	2825.0	3894.0	3894.9
LP_{sep} (KPa)	62.7	78.9	98.6	122.6	152.1	188.7	234.9	295.3	379.5	238.2

The results of the single and double-flash cycles are as expected. The thermal efficiencies and amount of work increase with reservoir temperature. The values calculated by the model match typical reported values for first law efficiency in the 5-15% range for the single-flash plant and 6-18% for the double-flash plant. An interesting result was that the first law efficiency for the double-flash fell below the single-flash plant at 360°C, when only the energy used by the cycle is considered. The solver found the optimum solution for the double-flash cycle at 360°C would have the high pressure separator operating at a pressure similar to the 340°C result, and a low pressure separator close to that of the 300°C result, which was not following the trend seen in the other results. The 360°C result is explored further in the discussion chapter of the paper.

The working fluids of binary closed-loop systems have such a large advantage over flashing technologies because of the ability to boil and run supercritical at substantially lower temperatures, and remain a saturated vapor over a

wider range of temperatures and pressures. That means each working fluid would have a temperature range where it's most effective; the result Figure 3.1 shows the specific power of each fluid as a function of temperature.

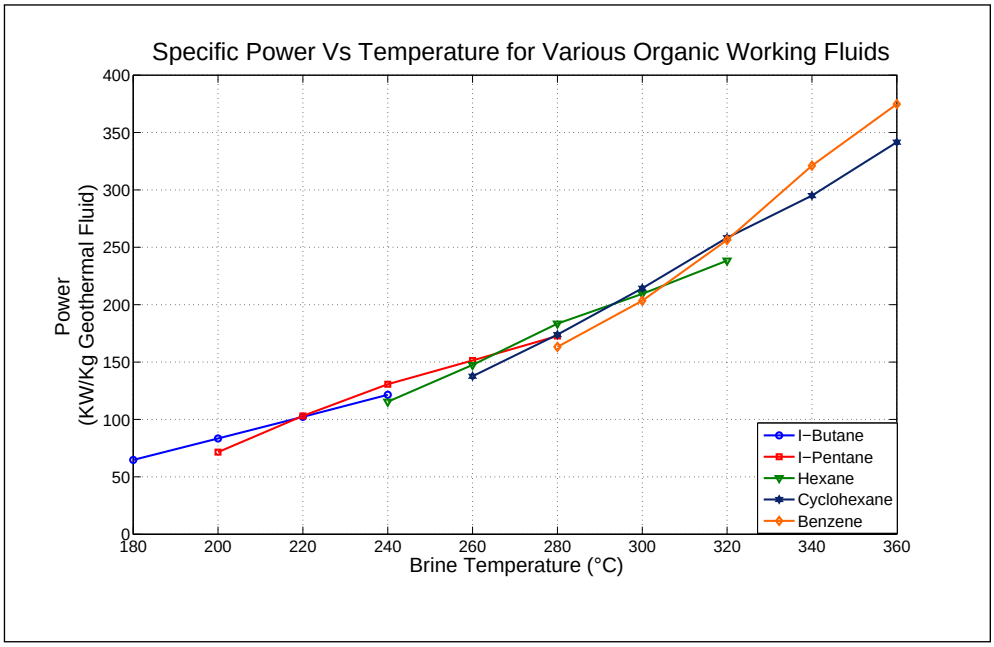

Figure 3.1: Specific Power Vs Temperature for Various Working Fluids.

In addition to the efficiencies listed for the flash cycle results, the binary cycles also measured η_{23} which is how efficient the cycle is on the working fluid side of the heat exchanger, which is an efficiency measure excluding exergy losses to the heat exchanger. Table 3.3 contains the optimal power output obtained from the best working fluid for that temperature. The solver chose to run the brine side at saturation pressure for all but the 300°C trial, in which it ran a two-phase mixture. This irregularity is further investigated in the disscussion chapter, and some possible causes are presented.

In addition to hydrocarbons, a trial with water as a working fluid was performed; the water was largely unsuccessful performing in between the single- and double-flash cycles. The results of the water trials are shown in Table 3.4 and are plotted along side the flashing cycles in Figure 3.2. Although the water trial did not perform as well as hoped, it did get some interesting solutions. In the low temperature ranges from 180-220°C it was choosing a sub-saturated cycle which was still meeting the quality constraints; after 220°C it was heating the vapor past saturation into the superheated region. It was the only fluid which the solver determined this solution to be optimal.

Table 3.3: Organic Rankine Cycle Results

Cycle	Reservoir Temperature (°C)									
Parameter	180	200	220	240	260	280	300	320	340	360
W(KJ/Kg)	64.75	83.45	103.06	130.69	151.40	183.44	214.27	258.30	321.11	374.79
E_d(KJ/Kg)	42.56	54.80	77.65	79.44	98.83	119.46	121.96	149.55	134.41	175.67
η_{11}(%)	8.73	10.04	11.17	12.86	13.59	15.09	16.18	17.92	20.41	21.53
η_{12}(%)	12.89	14.94	18.79	19.27	20.67	23.96	24.81	27.30	26.88	29.48
η_{21}(%)	38.77	41.05	42.71	45.90	45.96	48.01	50.49	51.52	55.93	55.74
η_{22}(%)	44.71	47.76	54.08	54.11	54.91	59.43	61.26	62.73	62.48	64.24
η_{23}(%)	46.97	49.83	56.10	56.17	57.66	61.18	62.65	64.20	63.94	65.64
Brine (KPa)	673.4	1143.3	1454.7	2447.7	2909.9	5110.2	2973.7	9572.6	12066	18666
ORC (KPa)	5159.3	7351.3	3528.5	6177.6	6424.3	5500.8	1949.5	6505.7	7433.3	11904
ORC Fluid	Iso-Butane	Iso-Butane	Iso-Pentane	Iso-Pentane	Iso-Pentane	Hexane	Cyclo-Hexane	Cyclo-Hexane	Benzene	Benzene

This approach is taken further in coal and nuclear plants where the fluid is often flashed and reheated numerous times in the superheated region before being condensed.

Table 3.4: Water Rankine Cycle Results

Cycle	Reservoir Temperature (°C)									
Parameter	180	200	220	240	260	280	300	320	340	360
W(KJ/Kg)	41.47	55.17	70.73	89.78	110.49	133.65	160.78	192.18	230.16	282.48
E_d(KJ/Kg)	68.47	79.84	97.44	133.25	154.46	177.02	193.31	218.23	245.14	274.78
η_{11}(%)	5.59	6.64	7.67	8.83	9.92	10.99	12.14	13.34	14.63	16.23
η_{12}(%)	12.04	13.76	15.63	16.16	18.11	19.90	20.30	21.29	23.53	24.97
η_{21}(%)	27.47	30.34	32.17	31.38	33.22	34.85	36.58	38.23	39.92	42.03
η_{22}(%)	43.48	46.88	48.95	42.54	45.26	47.52	47.33	49.30	50.94	52.32
η_{23}(%)	46.79	49.83	52.70	53.45	55.95	57.97	58.39	60.05	61.43	62.61

The Figure 3.2 is meant as a summary for visually comparing the plant modeling. It shows a clear advantage to using the binary cycles coupled with the correct working fluid, outperforming the flashing cycles over the entire temperature range.

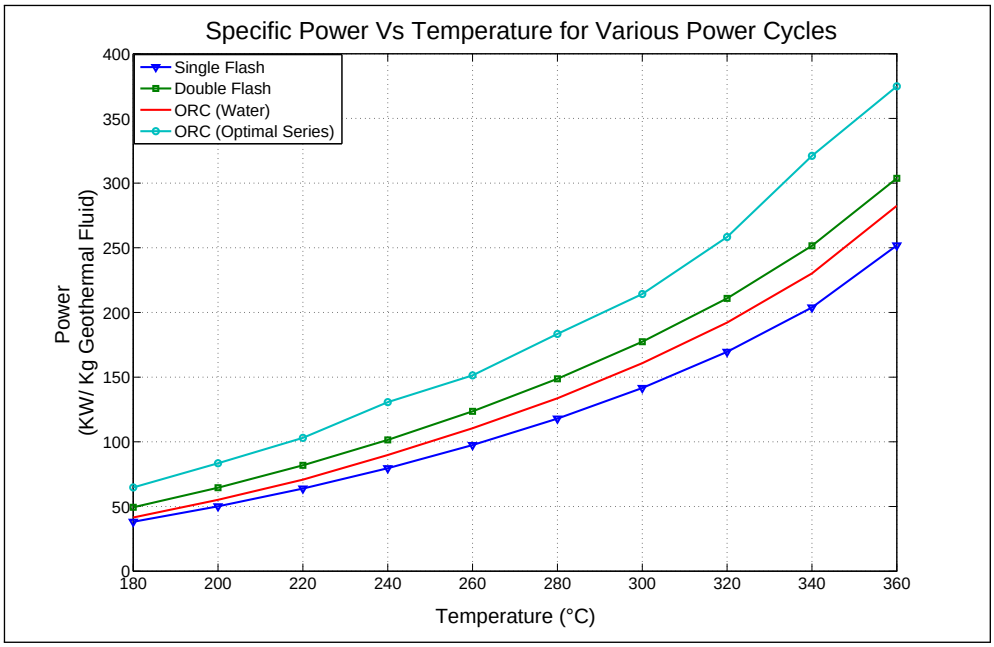

Figure 3.2: Specific Power production for Various Plant Types as a function of Temperature.

3.2 Wellbore Modelling Results

The results for the conventional wellbore modeling are shown in Figure 3.3. The pressure drop equations were applied to the same wellbore and reservoir at different mass flow rates to obtain the flowing wellhead pressures shown in the diagram. In the diagram, many of the fluid temperatures do not meet the vertical axis. This is because the wellhead pressure went into negative values at the higher mass flow rates. The negative values were assumed to represent a "no flow" condition. The flowing wellhead conditions also had to meet the criteria of being higher than the single- or double-flash separator pressures. This constraint meant the wells could not flow at their absolute open flow potential.

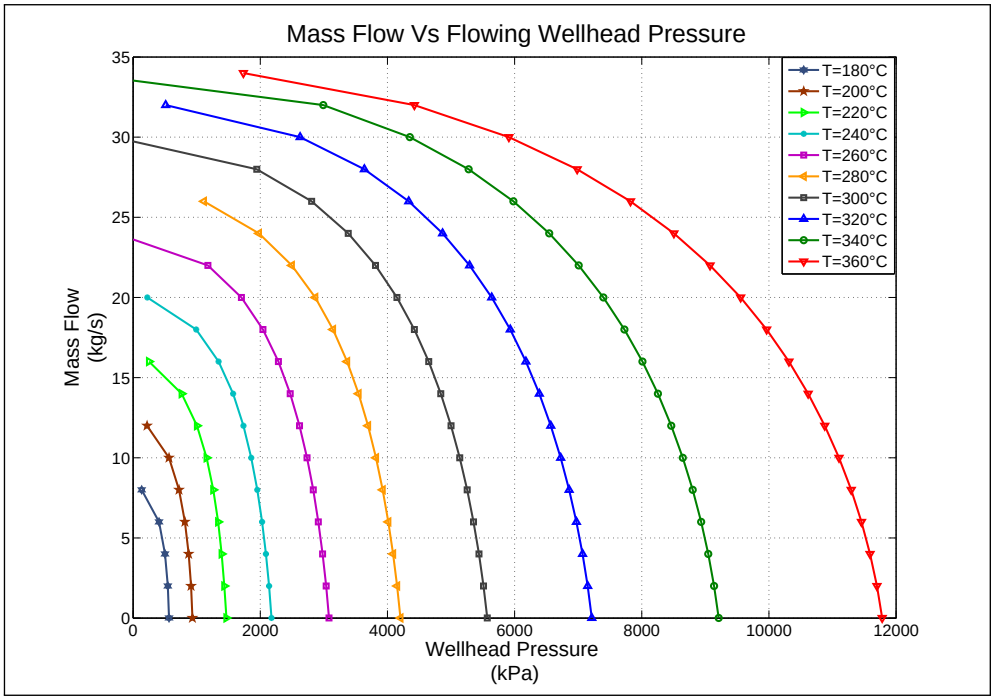

Figure 3.3: Estimated flowing wellhead pressures at various reservior temperatures and mass flow rates.

The mass flow modeling for the pumped wells was a bit more involved since there were more variables and constraints in the system. In addition to the pressure gradient, a pump setting depth had to be determined and a second gradient applied to account for the smaller production tubing. Unfortunately the pumps also had an inherent constraint on the setting depth. This was

encountered at temperatures over 300°C. It was found that in order to satisfy the studies'100m of hydraulic head on the pump suction constraint, the pump would have to be set deeper than the well. The boiling point of water at temperatures over 300°C would need wells significantly deeper to utilize downhole pumps. A similar occurrence was also noted when excessive drawdown in the higher temperature reservoirs lead to the formation of steam, these conditions would make pump use impractical or impossible.

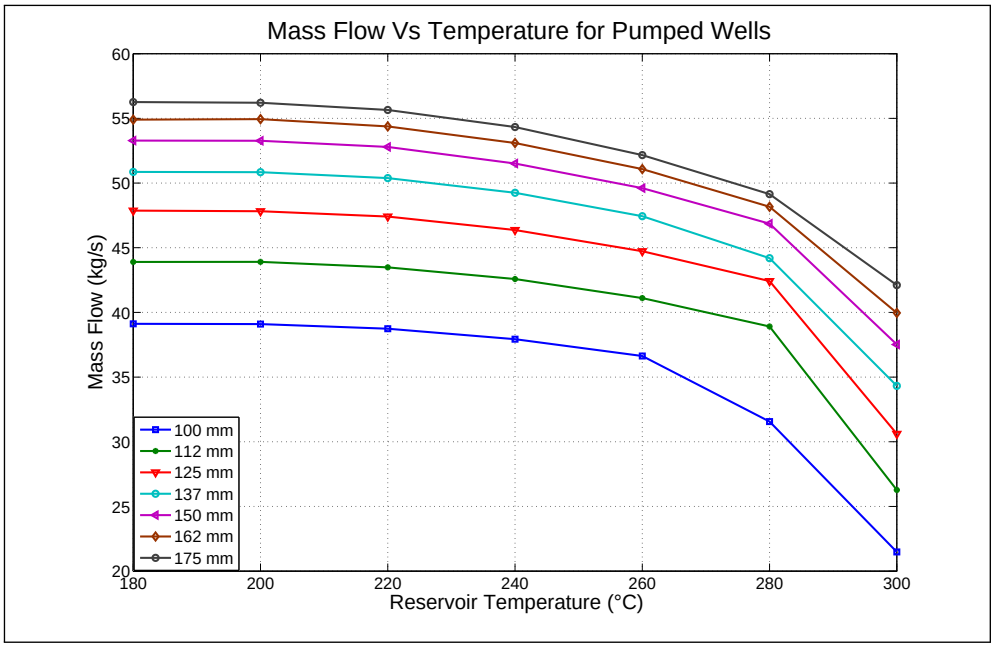

Figure 3.4: Estimated mass flow rates for various tubing diameters vs temperature.

The Figure 3.4 represents the optimal balance of pressure and flow rate for the well and plant system. In the plant and wellbore system the amount of useful work per kilogram of geo-fluid was balanced with the work provided by the pump until the best solution was found. The result was also seen when looking at the pump power consumption, which was maximized for nearly all data points.

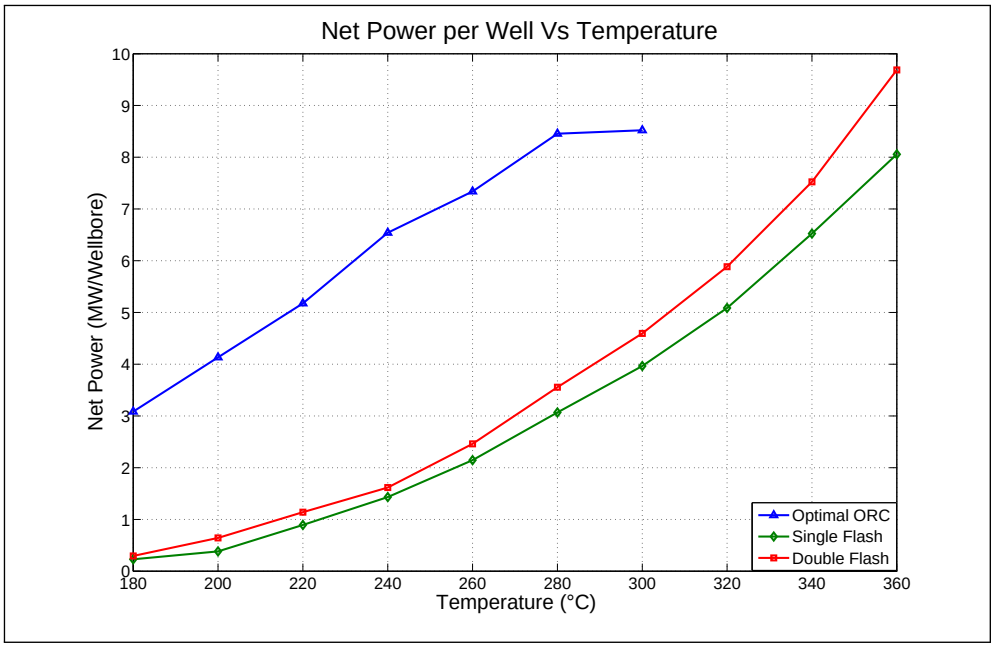

Figure 3.5: Net power output per wellbore for each technology.

The final result of combining the wellbore modeling with the power plant studies is shown in Figure 3.5. After obtaining expected values for mass flow from the two styles of well, we are able to estimate the amount of power that can be produced from each wellbore. The graph is based on the specific power capacity of each type of power cycle at a given temperature and was multiplied with the wellbores' mass flow at that given temperature. As mentioned previously, the pumps would not work at temperatures over 300°C, so no data is presented for temperatures over 300°C.

3.3 Economic Modelling Results

One of the background goals of the study was to allow smaller wellbores to be drilled if a single-phase fluid was to be used. Due to the huge variance present in nearly all drilling cost data, this proved difficult to make a decent comparison. The use of the production tubing did allow some indirect investigation, however. Figure 3.6 shows how the total wellbore cost, with tubing and pump costs included, changes as a function of production tubing diameter.

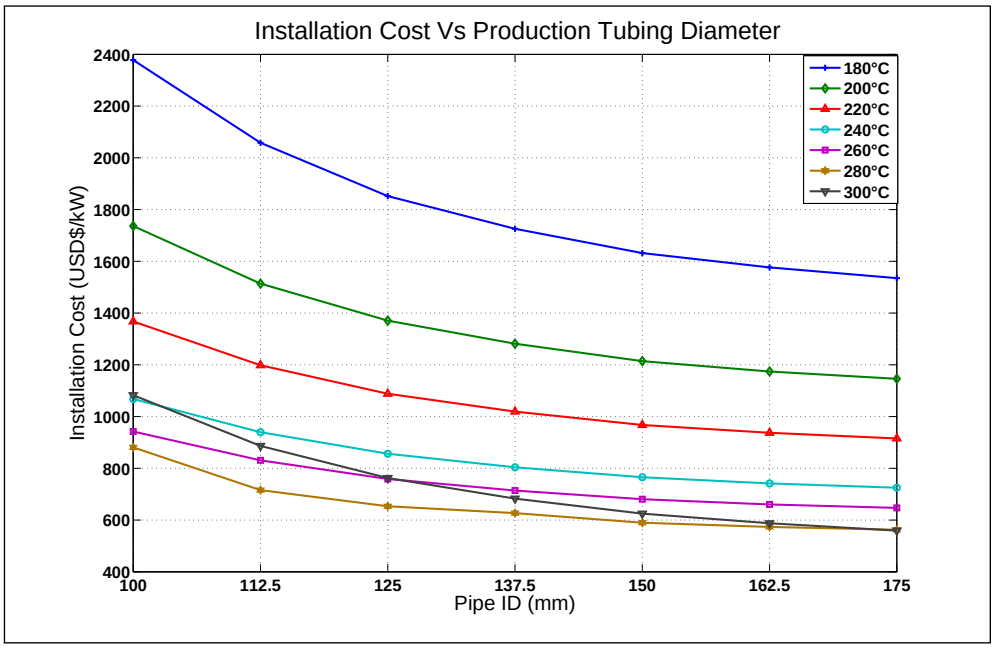

Figure 3.6: Installation costs for each temperature with various pipe diameters.

The installation costs for the binary wells all trended down with increased production tubing diameter, with the most dramatic differences being observed in the lower temperature reservoirs. Unfortunately the production tubing hit a diameter constraint in the wells' slotted liner, $7^{5/8}$ inch would be the largest diameter of standard casing that could be run with couplings. The lighter $7^{5/8}$ inch pipes have an inside diameter of 175mm which became the upper limit for the study. The trends did level out around this point in many of the higher temperatures indicating that an optimum diameter may be near this location. An interesting result from this modeling was that

the power production from a 280°C well would outperform the 300°C when tubing diameter was limited; this will be explained in further detail in the discussion section.

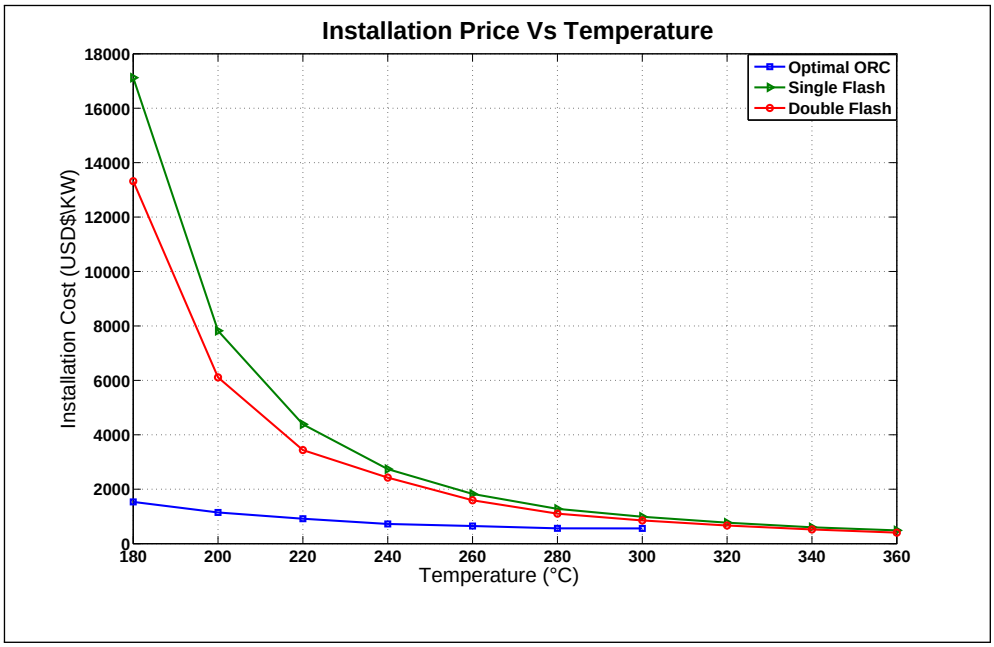

Figure 3.7: Installation costs for various technologies at different temperatures.

It is evident when looking at Figure 3.7 that installing flash technologies at low temperatures could be quite an expensive endeavor and likely will not be cost effective any time soon. The flashing costs do drop quickly, however, and the technologies could be considered comparable by around the 300°C region, especially when you consider the challenges associated with new technology and the extra maintenance required for the downhole pumps. Once again there is no data available for temperatures over 300°C, but it looks as though the technologies will become close to equal as temperatures approach 360°C.

While much focus in development is focused on installation costs, it can be beneficial to look at long term economic viability. In the economic model, maintenance, drilling and completion costs have been deducted from the revenue generated by the net power production sold at roughly 0.04 USD per kWh over the thirty-year period. The model assumed the pump and production tubing would be replaced every three years and the materials price and power price would remain constant over the thirty year period as

the year to year interest rate would keep at a constant five percent.

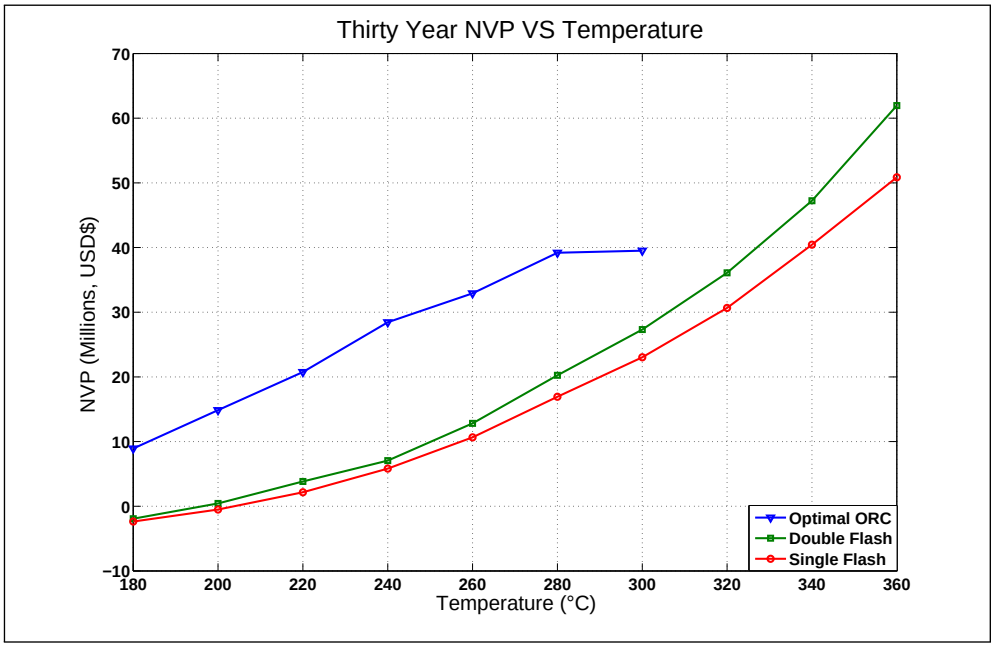

Figure 3.8: A thirty year net present value with the revenue and operational costs for pumped wells included.

The results of the economic model are shown in Figure 3.8, and depict the conditions where this technology is most advantageous over the flashing wells. While the Figure 3.8 has a similar profile to Figure 3.5, the two curves have moved closer together. The cost of replacing the pump and tubing had a negative impact on the previous advantage seen in Figure 3.5. The highest gains in returns are now seen in the 240°C to 280°C range. Once again, no data is available for temperatures over 300°C.

The graph also shows a negative value for the low temperature flashing technologies, which may be why there are not many low temperature flashing plants operating around the world. While the flashing technologies could work at 180°C they would be unprofitable at the power prices used in the study. The negative value seen in Figure 3.8 represents a net loss after 30 years of operation.

Chapter 4

Discussion

While the majority of the results did not require much interpretation, there were some non-intuitive results which may provide some insight into the questions not directly answered by the study. An original goal of the study was to investigate the possibility of slim wellbores as a cost saving measure, however, this was not a possibility due to a lack of available data. The production tubing and liner sizes can be indirectly be used to reverse engineer the surrounding wellbore. The production tubing installed with the downhole pumps shown in Figure 3.6 seemed to have a trend toward lower installation cost with an increase in pipe diameter. This result could indicate that it is cheaper to drill and install pumps on larger diameter wells rather than smaller diamter wells, however, one cannot say for certain without accurate cost figures. The previous work done by MIT [MIT, 2005], in Appendix A as Figure A.1, shows a power law trend as a function of depth. It is difficult to say with any certainty if diameter and drilling cost relationship would be similar to the trend seen in the depth and drilling cost relationship. If they did share a similar power law relationship, however, it would mean marginal increases in cost to add diameter to a well after a certain point.

The reservoir will also dictate the optimal diameter to some extent. A reservoir with a low productivity index does not need a large diameter well as it will not utilize the well to its full potential because of excessive draw down. A prolific reservoir with very little draw down, appears to favor larger diameter wells.

Although the curves in Figure 3.6 did not find an optimal pipe diameter,

the slope suggests the minimum installation cost may have been close to the 175mm pipe. This may also have been a function of the fixed wellbore depth, diameter and cost. In other words, the curves may indicate the efficiency gained in using the entire diameter of the well. Another trend seen in Figure 3.4 which supports the optimal flow rate conclusion is how the lines are getting closer together as the diameter increases, indicating diminishing returns as the tubing gets larger. The closing of the lines might suggests the bottle neck might be in the reservoir or pump. In the 300°C result shown in Figure 3.6 the rate was restricted in the smaller diameter pipes in order to meet the pressure constraints, and limited because of boiling in the reservoir in the larger diameter pipes. This meant more power could be extracted from the 280°C reservoir than the 300°C reservoir, until the larger tubing diameters were used.

A primary focus of the study was to investigate any advantages or efficiency gains when using saturated brine, as opposed to a two-phase mixture, for power generation. While the majority of the optimal solutions had working fluids in the supercritical region, the cyclo-hexane trial chose a saturated vapor solution. The saturated vapor solutions were seen with other fluids at temperatures below the critical temperatures. The saturated vapor solutions, however, were not outperforming the lighter molecular weight fluids running in supercritical conditions. The cyclohexane trials did go supercritical at the 320°C solution, which is slightly over the fluids' critical temperature of 316.65°C. The saturated vapor cyclohexane solution could be attributed to a missing working fluid which would fit between hexane and cyclohexane for molecular weight and boiling point. A fluid like hexene, or another six carbon molecule with double or triple bonds, might have outperformed the sub-saturated cyclohexane. Another possibility could be that the temperature profiles of the brine and cyclo-hexane sides of the heat exchanger fit together to maintain the pinch tolerance, but destroyed minimal exergy in the heat transfer process.

In the results section, mention was made of the single-flash cycle outperforming the double flash cycle in the 360°C trial when energy lost to reinjection was taken into account in the calculation of η_{12}. A second derivative curve of the specific work for both cycles was plotted and it was found that the single-flash does indeed increase its rate of power generation more that the double-flash over the 340°C-360°C interval. It is possible the flashing cycles can utilize the steam better through a single turbine as the temperature approaches the critical temperature of water, and the second flashing stage may become less necessary as the amount of the liquid phase in the separator

diminishes. The diminishing liquid phase in the separator could also explain why the solver found similar high pressure separator conditions optimal in both the 340°C and 360°C trials, promoting a higher mass fraction into the high pressure turbine. The low pressure in the secondary separator produced 25% steam quality which resulted in a mixture of 91% quality for the low pressure turbine. While the low pressure turbine still produced more work due to its higher mass flow than the high pressure turbine, the trend would indicate the high pressure turbine will overtake the low pressure turbine for work output. The results indicate that as temperatures approach the critical temperature of water, the secondary flashing unit can reduce first order efficiency if the reinjection energy is not included. The double-flash process still creates more energy because it utilizes more of the fluids' energy than the single-flash process by flashing it twice, while the resulting cycle efficiency excluding re-injection η_{11} is higher, the efficiency including re-injected energy η_{12} is lower.

The power plant models compared fairly well to the previous work done in the field. During the modeling process much care was taken to ensure the different plant models where yielding correct and possible solutions over the range of temperatures examined. In his study Mortaza Yari [Yari, 2009] had used brine temperatures of 230°C for his study of flashing technologies; while they were not explicitly expressed in my results, the values for available work presented in that study fit between the surrounding data points of the current study. The exergy destruction rates reported in the Yari study are lower than the models used in the current study obtained. This could be due to the cooler condenser temperatures, which would yield higher thermal efficiencies, or the dead state temperature of 25°C, as opposed to the 5°C used in my study. The dead state temperature is involved in the calculation of all of the exergy relations, and it could be enough to reflect the differences present in the results.

The results for the ORC cycles had a common temperature of 180°C between this study and [Yari, 2009], however, the studies had different working fluids. The values presented in the Yari study obtained lower specific work and higher exergy destruction. This could be due to the choice of working fluids or the choice not to run them in supercritical conditions. Both studies had saturated brine. The values obtained for the primary second law efficiencies are nearly the same, although η_{22} and η_{23} are quite a bit higher in the Yari study. This may be a result of the working fluids properties, the dead state temperature or a combination of both.

A paper done by GeothermEx [Sanyal, 2007] found that a pumped well cannot deliver more than 7.3MW net power regardless of productivity index and that there was little to gain by raising the operating temperature limit of commercially available pumps. This study had some very different assumptions than the current study, and could give the assumption to most readers that it is better to run flash cycles after 190°C. The study fixed the pump setting depth to 457m (1500 feet) which is the maximum setting depth of most shaft driven pumps. The authors of the GeothermEx paper did in fact encounter the same problem this study encountered at temperatures over 300°C; cavitation occurring at the pump suction due to the higher pressures required to prevent boiling in hotter fluids. In fact the current study found that the 280°C reservoir for most tubing diameters could produce more power than the 300°C reservoir due to boiling constraints.

The study from GeothermEx does in fact provide a graph early in the paper which suggests there is no practical upper limit on power per well if the pump can be set deep enough to prevent cavitation. Results from the current study support this statement, as no limits on gross power per well were encountered until the well bottom of 2500m. The net power per well will eventually hit an additional constraint in the form of discharge pressure or pressure losses due to friction as depth increases. While the GeothermEx paper takes a very practical approach to the downhole pumps, the results and limitations encountered in both studies seem to revolve around pump cavitation at high temperatures.

The Lemelson report [Foundation for Geothermal Innovation, 2009] looks at the pump development on a very big scale; the report includes social, economic and technical changes associated with line shaft pump and current electronic submersible pump technology. While much of the report is outside the scope of the study, the report does provide some speculated geothermal potential for various parts of the world. The gains are meant to reflect the additional resources which would be accessible to producers if pumps could be installed at depths greater than 335m (1100 feet) which is the limit they put on line shaft pumps. The outcome is surprising to say the least; they predict roughly 10 fold increases in capacity for nearly all regions and in some cases more. In Iceland, for example, they predict the current installed capacity of 490MW would have a potential of 5800 MW. The results from this study would seem to suggest it would likely be 2-3 times the power output, not 10. The Lemelson report may be including resources not currently developed using existing technology in the estimates by area as well.

The challenges encountered during the study came largely from the financial modeling in the form of information availability and reliability. Geothermal power developers tend to keep the costs associated with various activities secretive, and it's difficult to gauge the accuracy of third or often fourth hand cost figures. In an effort to reduce the impact the financial variations would have on the study of power generation, many costs between the two production methods were assumed equal. In all likelihood the wells producing via production tubing would require less maintenance on the wellbore above the fluid level since there is no flow in that annulus. The wellbore liners should see similar amounts of wear regardless of the production method unless boiling was occurring in the liner for the two-phase case. The rest of the financial comparison is based on first hand tubing costs and the Lemelson reports' estimate for what this new pump would cost, as those figures came from the people who would likely be building the new pumps.

The study also pays no attention to gathering systems, transmission lines, or any other plant-specific costs not related directly to the wellbores and pumps. The idea behind avoiding a sensitivity analysis of the plant was simply due to the fact that all the assumptions and costs would likely be more incorrect than meaningful. A complete sensitivity analysis is arguably outside the scope of interest, and would have been primarily estimates and guess work rather than solid cost figures.

An unforeseen problem encountered in the study was the pump cavitation discussed earlier. While it was easier to set the drilling costs equal for a 2500m well, it did introduce the pump setting depth problem. It would have been relatively easy to use a 3000m or deeper well to ensure that the pump could be set deep enough to prevent suction cavitation; but it would be impractical for the lower temperature reservoirs and would have not changed the two-phase well case. Ultra deep wells may not be needed in hydrothermal fields, as they are in conventional EGS fields, as naturally occurring fractures can be used to conduct fluids from deeper in the earth to the pumps.

The study was one of the first to take a new approach to a previously existing technology. The contribution to the field is unlocking the potential of modern production techniques and applying them correctly to the right reservoirs. The engineers who built Magmamax knew that steam was a poor pump and installed the downhole pumps available to them at the time; both the pumps and applications can be improved.

Chapter 5

Conclusions

Results of the study suggest that the use of downhole pumps in high temperature hydrothermal systems could lead to significant gains in power production, and potentially reduce the number of wells required to develop or sustain an existing geothermal field, thus reducing development costs. The advantages of pumping disappear as the critical temperature of water is approached, due to an increase in well productivity and improved performance from the flashing cycles. Additional benefits of the downhole pumps could be a reduction of the social and environmental impacts of geothermal development in sensitive areas by leaving a smaller surface footprint than flashing technologies.

The literature review did find other studies regarding optimizing pump setting depth and the benefits of downhole pump use; however, the previous work was limited to relatively shallow applications and lower temperatures [Sanyal, 2007], [Hinrichs, 1980]. The results would suggest that well depths for these pumped hydrothermal wells will have to be governed by temperature and suction pressure rather than fracture locations and productivity index alone. Pump cavitation may seem like a trivial challenge to overcome, poor well planning or hotter-than-anticipated reservoir fluids could add additional workover and drilling costs if not addressed properly.

While the study compared various types of power plants and two types of well bore production, the study failed to use downhole pumps with the flashing cycles. While it's doubtful the flashing cycles would have outperformed the organic Rankine cycles, the investigation might be of interest for developers

with existing flashing plants. The pumps would still improve the mass flow per well and would not have to maintain saturation pressure, so much less power would be required to run this configuration, and it would be a relatively low risk trial to add such a pump to an existing wellbore built for two phase flow.

In terms of future work, this study was limited in scope to some extent by data availability regarding drilling costs as a function of diameter and depth. This factor makes comparisons and improvement difficult; many developers are using identical wellbore designs. The costing for such a study is trivial, however estimating or trending drilling parameters such as rate of penetration with diameter would be essential to evaluating accurate costs for diameter and depth.

The study investigates the practice of pumping deeper and hotter wells, but stops short of supercritical formation fluids, such as those encountered during the Iceland Deep Drilling Project (IDDP). This begs the question; could a downhole pump be used for supercritical fluids? And if so, what challenges would be associated with its implementation?

The current study has relevance to modern developers who will have to fill the energy void left by diminishing oil reserves and an emerging third world appetite for energy. The geothermal developers of the future will also have to be more environmentally conscious in addition to keeping the costs affordable for consumers. While this study is by no means comprehensive, it may provide a basis for further investigation into the topic and potentially lead to the necessary incentive required to advance downhole pump technology and improve utilization.

Bibliography

Axelsson, G. (2009). Geothermal Reservoir Engineering: University of Iceland Spring 2009 [PDF document]. Lecture notes from the course Geothermal Systems, Recieved in March 2009.

Beggs, H. D. (2003). Production Optimization Using Nodal Analysis. Tulsa, Oklahoma, USA: OGCI and PetroSkills

Bodvarsson, G.S., & Witherspoon, P.A. (1989). Geothermal Reservoir Engineering Part 1. Geothermal Science and Technology, 2, 1-68.

DiPippo, R. (2008). Geothermal Power Plants: Principles, Applications, Case Studies and Enviromental Impact. Kidlington, Oxford, GB: Butterworth-Heinemann publications.

The Foundation for Geothermal Innovation. (2009). Designing A Global Geothermal Challenge "The Lemelson Report". California, USA: The Foundation for Geothermal Innovation.

Geothermal Energy Association. (2005). Factors Affecting Costs of Geothermal Power Development. Washington, D.C., USA: Geothermal Energy Association.

Hanna, E., Jónsson, T., Box, J.E. (2004). An analysis of Icelandic climate since the nineteenth century. International J. of Climatology 24, 1193-2004.

Hinrichs, T. C., & Dambly, B. W. (1980). Proceedings of the Fourth Annual Geothermal Conference and Workshop, Electric Power Research Institute, TC-80-907-23. Palo Alto, California, USA.

Khalilabad, M.R. & Axelsson, G. 2008. Proceedings from Thirty-Third Workshop on Geothermal Reservoir Engineering. Stanford, California, USA: Stanford University.

Lemmon, E.W., Huber, M.L., McLinden, M.O. NIST Standard Reference Database 23: Reference Fluid Thermodynamic and Transport Properties-REFPROP, Version 8.0, National Institute of Standards and Technology, Standard Reference Data Program, Gaithersburg, 2007.

The Mathworks Inc., Natick, MA, (2007). MATLAB 7.7.0 (R2008b)[Software]. Available from http://www.mathworks.com/

Massachusetts Institute of Technology. (2005). The Future of Geothermal Energy: Impact of Enhanced Goethermal Systems (EGS) on the United States in the 21st Century. Retrieved from http://www1.eere.energy.gov/geothermal/future_geothermal.html

Pálsson, H. (2009). Utilization of Geothermal Energy for Power Production [PDF document]. Lecture notes from the course Design of Geothermal Power Plants, Received in September 2009.

PHYWE SYSTEME GMBH., 37070 Göttingen, Germany,(1998). Surface tension by the ring method (Du Nouy method). Retrieved from http://www.nikhef.nl/~h73/kn1c/praktikum/phywe/LEP/Experim/1_4_05.pdf

Sanyal, S. (2004). Cost of Geothermal Power and Factors that affect it. Richmond, California, USA: GeothermEx, Inc.

Sanyal, S. K., Morrow, J. W., & Butler, S. J. (2007). Proceedings from Thirty-Second Workshop on Geothermal Reservoir Engineering. Stanford, California, USA: Stanford University.

Schuster, A., Karellas, S. & Aumann, R. (2010). Efficiency optimization potential in supercritical Organic Rankine Cycles. Energy, Vol 35, PP. 1033-1039.

Storn, R. & Price, K., (March 1995). Differential Evolution-A simple and effective adaptive scheme for global optimization over continuous spaces. Technical Report TR-95-012, ICSI, March 1995. Retrievedfromhttp://www.icsi.berkeley.edu/~storn/litera.html

Towler, B. (2002). Fundamental Principles of Reservoir Engineering, Richardson, Texas: Society of Petroleum Engineers

Yari, M. (2009). Exergetic analysis of various types of geothermal power plants. Renewable Energy, 35(2010), 112-121.

Appendix A

The following tables are a round of sample calculations performed at 240 °C for each of the power cycles presented in the methods and materials section. The table's values correspond to a point or node in the cycle, and the parameters used to calculate such things as work, exergy, and mass flows required to balance the energy in the cycle.

Table A.1: Single Flash Cycle

Single-flash process with a reservoir temperature of 240 °C						
Node Number	Fluid Type	Pressure P(kPa)	Temperature T(°C)	Mass Flow $\dot{m}$(kg/s)	Enthalpy h(kJ/kg)	Entropy s(kJ/kg.K)
0	Geofluid	3347	240	1	1038	2.702
1	Geofluid	348.6	138.7	1	1038	2.828
2	Geofluid	348.6	138.7	0.2113	2732	6.942
3	Geofluid	9.595	45	0.2113	2355	7.449
4	Geofluid	9.595	45	2.947	188.4	0.639
5	Water	100	5	2.736	21.12	0.076

Table A.2: Double Flash Cycle

Double-flash process with a reservoir temperature of 240 °C						
Node Number	Fluid Type	Pressure P(kPa)	Temperature T(°C)	Mass Flow $\dot{m}$(kg/s)	Enthalpy h(kJ/kg)	Entropy s(kJ/kg.K)
0	Geofluid	3347	240	1	1037.6	2.702
1	Geofluid	828.27	171.85	1	1037.6	2.757
2	Geofluid	828.27	171.85	0.1519	2769.7	6.650
3	Geofluid	123.74	105.67	0.1519	2540.9	6.909
4	Geofluid	123.74	105.67	0.2594	2600.4	7.066
5	Geofluid	9.595	45.00	0.2594	2343.3	7.412
6	Geofluid	9.595	45.00	3.6001	188.4	0.639
7	Geofluid	828.27	171.85	0.8481	727.2	2.060
8	Geofluid	123.74	105.67	0.8481	727.2	2.121
9	Geofluid	123.74	105.67	0.1075	2684.4	7.287
10	Water	100	5.00	3.3413	21.12	0.076

Table A.3: Organic Rankine Cycle

Organic Rankine Cycle with a reservoir temperature of 240 °C						
Node Number	Fluid Type	Pressure P(kPa)	Temperature T(°C)	Mass Flow $\dot{m}$(kg/s)	Enthalpy h(kJ/kg)	Entropy s(kJ/kg.K)
0	Geofluid	3346.9	240.00	1.000	1037.6	2.7020
1	I-Pentane	176.93	45.00	1.592	40.16	0.1293
2	I-Pentane	6177.6	47.82	1.592	51.31	0.1328
3	I-Pentane	6177.6	80.02	1.592	130.12	0.3667
4	I-Pentane	6177.6	n/a	1.592	n/a	n/a
5	I-Pentane	6177.6	217.68	1.592	556.04	1.3725
6	I-Pentane	176.93	93.73	1.592	462.80	1.4371
7	I-Pentane	176.93	52.82	1.592	383.99	1.2095
8	Geofluid	2447.7	222.83	1.000	1037.6	2.7069
9	Geofluid	2447.7	n/a	1.000	n/a	n/a
10	Geofluid	2447.7	85.38	1.000	359.49	1.1374
11	Water	100.00	5.00	3.736	21.12	0.0763
12	Water	100.00	40.00	3.736	167.62	0.5724

Table A.4: Organic Rankine Cycle with Water

ORC with Water and a reservoir temperature of 240 °C						
Node Number	Fluid Type	Pressure P(kPa)	Temperature T(°C)	Mass Flow $\dot{m}$(kg/s)	Enthalpy h(kJ/kg)	Entropy s(kJ/kg.K)
Reservoir	Geofluid	3346.9	240.00	1.000	1037.6	2.702
1	Water	9.595	45.00	0.202	188.43	0.639
2	Water	254.71	45.01	0.202	188.71	0.639
3	Water	254.71	128.03	0.202	2717.3	7.046
4	Water	254.71	234.99	0.202	2939	7.537
5	Water	9.595	45.00	0.202	2494.3	7.886
6	Geofluid	3346.9	240.00	1.000	1037.6	2.702
7	Geofluid	3346.9	230.53	1.000	992.77	2.614
8	Geofluid	3346.9	114.32	1.000	481.99	1.464
9	Water	100.00	5.00	3.736	21.12	0.076
10	Water	100.00	40.05	3.736	167.62	0.572

A.1 Previous Economic Studies

Table A.5: Capital cost of geothermal power technologies. Adapted from [Geothermal Energy Association, 2005].

Author	Technology	Capital Cost ($/kWh)	Capital Cost Range ($/kWh)	Inflation adjusted capital cost (2010$)
Entingh & McVeigh (2003)	Binary	2400	1700 - 2700	2844
CEC, RRDR (2003)	Binary	2275		2697
CEC, CCCCSEGT (2003)	Binary	2293		2717
Owens (2002)	Binary	2112		2560
Kutscher (2000)	Binary	2100		2659
EPRI (1997)	Binary	2112		2869
Average Capital Cost Binary		*2215*	*1700-2700*	*2724*
CEC, RRDR (2003)	Flash	1950		2311
CEC, CCCCSEGT (2003)	Flash	1911		2265
Owens (2002)	Flash	1444		1750
Stefanson (2002)	Flash	1750	1062-1992	2122
Kutscher (2000)	Flash	1450		1837
EPRI (1997)	Flash	1444		1962
Entingh & McVeigh (2003)	D.Flash	1800	1500 - 2400	2136
Entingh & McVeigh (2003)	S.Flash	1500	1200 - 1800	1777
Average Capital Cost Flash		*1656*	*1062-2400*	*2020*

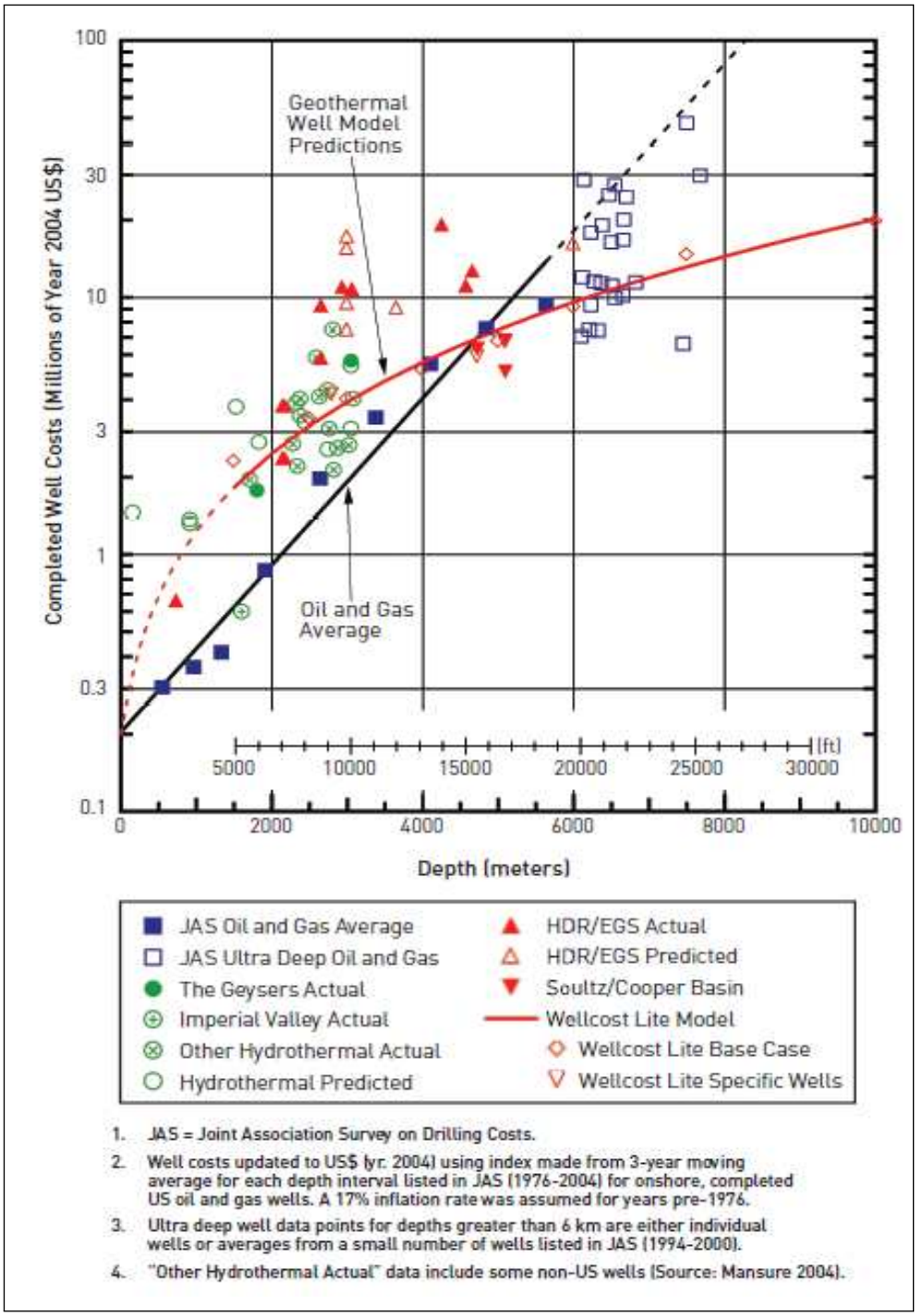

Figure A.1: Completed well costs for Oil,Gas and Geothermal wells in 2004 U.S.$. [MIT, 2005]